# Velocity-Assisted Predictive Mobility and Location-Aware Routing Protocols for Mobile *Ad Hoc* Networks

Kai-Ten Feng, *Member, IEEE*, Chung-Hsien Hsu, *Student Member, IEEE*, and Tse-En Lu

***Abstract*—In recent years, many location-aware routing protocols have been proposed for mobile *ad hoc* networks. The efficiency of the routing protocols can be improved by considering the location information of the mobile nodes (MNs). However, the mobility characteristics of the MNs have not been taken into account in most of the related work. In this paper, the proposed velocity-aided routing (VAR) algorithm determines its packet-forwarding scheme based on the relative velocity between the intended forwarding node and the destination node. The routing performance can further be improved by the proposed predictive mobility and location-aware routing (PMLAR) algorithm, which incorporates the predictive moving behaviors of MNs in protocol design. The region for packet forwarding is determined by predicting the future trajectory of the destination node. The routing performance can be effectively enhanced by adopting both the proactive maintenance and the VAR mechanisms within the proposed PMLAR scheme. Simulation results show that the PMLAR protocol associated with its derivative schemes outperforms other routing protocols under different network topologies.**

***Index Terms*—Location-based *ad hoc* routing protocol, Mobile *Ad hoc* NETwork (MANET), mobility model, prediction mechanism.**

## I. Introduction

A MOBILE *Ad hoc* NETwork (MANET) consists of wireless mobile nodes (MNs) that cooperatively communicate with each other without the existence of a fixed network infrastructure. Depending on different geographical topologies, the MNs are dynamically located and continuously changing their locations. The fast-changing characteristics of MANETs make it difficult to discover routes between MNs. It becomes important to design efficient and reliable routing protocols to maintain, discover, and organize the routes in MANETs. Recent interest in the design of *ad hoc* routing algorithms include applications for the military, intervehicle communication, personal communication services, and sensor networks.

Manuscript received January 9, 2006; revised August 10, 2006 and February 25, 2007. This work was supported in part by the National Science Council under Grant 92-2218-E-009-018, the MOE ATU Program 95W803C, and the MediaTek Research Center, National Chiao Tung University. The review of this paper was coordinated by Prof. A. Ganz.

K.-T. Feng and C.-H. Hsu are with the Department of Communication Engineering, National Chiao Tung University, Hsinchu 300, Taiwan, R.O.C. (e-mail: ktfeng@mail.nctu.edu.tw; chhsu.cm94g@nctu.edu.tw).

T.-E. Lu is with Alpha Networks Inc., Science-based Industrial Park, Hsinchu 300, Taiwan, R.O.C. (e-mail: jnlu.cm92g@nctu.edu.tw).

Color versions of one or more of the figures in this paper are available online at http://ieeexplore.ieee.org.

Digital Object Identifier 10.1109/TVT.2007.901897

A number of *ad hoc* routing protocols have been developed for MANETs. The topology-based routing protocols can be categorized into proactive (such as destination sequence distance vector [1] and wireless routing protocol (WRP) [2]) and reactive algorithms (such as *ad hoc* on-demand distance vector routing [3], dynamic source routing (DSR) [4], temporally-ordered routing algorithm (TORA) [5], associativity-based routing (ABR) [6], and signal stability based adaptive routing [7]). The proactive routing protocols periodically maintain tables at each MN. The routing tables record persistent and up-to-date information within the changing network topologies. The proactive algorithms offer reliable routing information between the MNs, while the overhead for maintaining the routing tables can be rapidly increased as the expansion of the MN's numbers and mobility within the network. The reactive algorithms initiate route discovery processes based on the request from the source node. The routing tables are only maintained within the requested routes from the source to the destination nodes. The on-demand characteristics of the reactive algorithms generate less routing overhead compared with the proactive routing protocols. However, additional delay has been incurred by the route discovery processes within the reactive algorithms.

The hybrid routing approaches (such as zone routing protocol (ZRP) [8], [9], clusterhead gateway switch routing (CGSR) [10], [11], and core extraction distributed *ad hoc* routing algorithm (CEDAR) [12]) compromise the benefits between proactive and reactive algorithms. ZRP utilizes the proactive-based approach within its predetermined local area, while the reactive algorithm is adopted outside the area. Cluster heads (as in CGSR) or cores (as in CEDAR) are selected from the MNs to serve as gateways for information distribution within the network. The hybrid approaches can be utilized to adopt themselves by considering the tradeoffs between the communication reliability and the routing overhead. The performance comparison between the various types of *ad hoc* routing protocols has been conducted in several studies, as in [13]–[16].

There are increasing interests in the design of location-based *ad hoc* routing algorithms [17]–[25]. With the prosperity of mobile devices equipped with positioning systems (such as global positioning systems [26]), it becomes feasible to utilize the location information from mobile devices in routing protocol design (such as distance routing effect algorithm for mobility (DREAM) [20], location-aided routing (LAR) [21], geographical routing algorithm (GRA) [22], greedy perimeter stateless routing (GPSR) [23], and grid location service (GLS) [24],

[25]). The DREAM protocol proactively distributes the location information of each MN within the network. The data packets are delivered from the source node to the destination node based on the built-in location database within each MN. On the other hand, the LAR protocol is a reactive location-based algorithm. The route discovery and packet-forwarding region is restricted within a predetermined area based on the knowledge of the MN's location. The routing overhead can therefore be reduced by the directional flooding scheme proposed in the protocol.

As indicated in the survey on position-based routing algorithms [27], the location services and the packet-forwarding strategies are the two major components in on-demand routing protocol design. The primary purpose of location services is to provide the position information of the destination node to the source node for its packet delivery. Based on the information, the position-aware routing protocols can determine their route discovery and packet-forwarding strategies. Most of the position-aware routing protocols utilize global flooding [20]–[22] as their location services, which results in excessive amounts of control packet overhead. The algorithm alleviates the problem by providing location updates within the local area of the network. A small set of MNs serves as the location server that offers location information for their neighborhood MNs. The appropriate selection of the location servers influences the performance of the location updates within the GLS scheme. A comparative study between the location-based *ad hoc* routing protocols can be obtained as in [28] and [29].

On the other hand, different types of MN mobility models have been studied in the previous research works [30]–[32]. It has been observed and demonstrated that the mobility models utilized in the *ad hoc* network simulations greatly influence the effectiveness of the routing algorithms. The commonly used random waypoint mobility (RWM) model (as was utilized in [13] and [14]) has been found to be insufficient in most of the realistic scenarios [33]. Different types of mobility models have been proposed to emulate the motion behaviors of MNs. It is suggested that the designed *ad hoc* routing protocols should be evaluated under the various types of MN mobility models to satisfy the requirements for realistic circumstances.

However, the mobility patterns of the MNs have not been taken into consideration in most of the location-based routing protocol design. Since the velocity and heading angle of the MN are obtainable from positioning systems, it is practicable to incorporate the information in the design of *ad hoc* routing protocols. The proposed velocity-aided routing (VAR) algorithm determines its packet-forwarding scheme by calculating the relative velocity between the potential forwarding nodes and the destination node. This scheme forwards the data packets via those intermediate nodes that are faster approaching the destination node. The Gauss–Markov mobility (GMM) model [34], [35] and the constant speed mobility (CSM) model are utilized in the design of the VAR algorithm to calculate the MN's speed and moving angle. The benefit of using the GMM model is that it can be utilized to adaptively emulate possible moving behavior with certain levels of linear and Brownian motions. It will be shown in this paper that the proposed VAR algorithm is especially feasible for topologies with confined shapes and dynamic characteristics (e.g., highways or city streets). It will also be illustrated in the simulation results that the VAR algorithm based on the GMM model provides better routing performance compared with that based on the CSM model.

Moreover, since the mobility of the MNs is diverse under different moving scenarios, it will be beneficial to incorporate the MN's predicted movement in the design of routing protocols. The proposed predictive mobility and location-aware routing (PMLAR) protocol determines its packet-forwarding scheme by predicting the future position of the destination node. The prediction mechanism defines the packet-forwarding region by adapting its adjustable parameters based on the previous moving behavior of the destination node. The GMM model is utilized as the prediction model in the design of the PMLAR algorithm, where its tunable parameters are adjusted with online adaptation. There are three additional enhanced schemes associated with the PMLAR algorithm. The PMLAR-V scheme incorporates the VAR algorithm to consider the relative velocities between the MNs within the route discovery process. The PMLAR-LV method further encompasses the local repairing mechanism within the PMLAR-V scheme. Furthermore, the PMLAR-PV scheme enhances the routing performance by exploiting both the VAR algorithm and the mechanism for proactive maintenance. It will be shown in this paper that the proposed PMLAR algorithm with its derivative schemes is feasible for different types of network topologies. Three mobility models, i.e., the highway mobility (HM) model, the RWM model, and the RWM model with indirect route (RWM-IR), are implemented in the simulations to provide different types of simulation scenarios. The effectiveness of the proposed VAR, PMLAR, PMLAR-V, PMLAR-LV, and PMLAR-PV algorithms is evaluated and compared with other existing routing protocols via simulations.

The remainder of this paper is organized as follows: Section II-A and B review and reformulate the existing DSR and LAR protocols. The two predictive mobility models, i.e., the GMM and CSM models, are presented in Section III-A. Section III-B explains the proposed VAR algorithm based on the two predictive mobility models. The proposed PMLAR protocol and its derivative schemes are presented in Section IV. The mobility models for simulation purposes, including a feasible HM model, are developed and introduced in Section V-A. The simulation parameters are defined in Section V-B. The parameter estimation for both RWM and HM models is conducted in Section V-C, while the performance evaluation of the proposed routing protocols is demonstrated Section V-D. Section VI draws the conclusions.

## II. Preliminaries

In this section, two on-demand routing protocols, i.e., the DSR and LAR algorithms, are reviewed. These two protocols provide the baseline route discovery and data transmission mechanisms for the proposed PMLAR protocol. Both protocols will be analyzed and compared with the PMLAR algorithms in the simulations. The route discovery and packet-forwarding

strategies of the DSR and LAR protocols are summarized as follows.

### A. DSR Protocol

The DSR protocol [4] is a source-initiative on-demand routing algorithm. The source node $S$ intends to send data packets to the destination node $D$ via some of the forwarding nodes $N_i$. $S$ will first check its route cache to verify if there are existing routes to the destination node $D$. If there is no such route in the cache, $S$ will start a route discovery process by broadcasting a route request $(RREQ)$ packet. The addresses of $S$ and $D$ are both written in the route record in the $RREQ$ packet header. Upon receiving the $RREQ$ packet, the intermediate node $N_i$ will rebroadcast the packet if the route to $D$ is not available. $N_i$ will also add its own address to the route record in the $RREQ$ packet. Until the destination node $D$ is found in the route discovery process, a route reply $(RREP)$ packet, which contains the complete route information from $S$ to $D$, is sent back to the source node $S$. The source node $S$ will utilize the constructed route to initiate data transmission to $D$.

### B. LAR Protocol

The LAR protocol is also an on-demand routing algorithm [21]. With the assistance of the MN's position information, the algorithm restricts the packet flooding area in the route discovery process instead of spreading out to the whole region as in the DSR protocol. The position information of the destination node $D$ is assumed available by the source node $S$ in the LAR protocol. One of the commonly used LAR algorithms, which is called the LAR-Box, defines a rectangular region for packet forwarding named the *Request Zone*. The circle, which is called the *Expected Zone* in the LAR-Box algorithm, is centered at the destination position $P_D(t_p)$, where $t_p$ represents a previous time instant that the location information of $D$ was acquired by $S$. The radius of the *Expected Zone* $(R_l)$ is determined by $S$ at the current time instant $t_c$, which is defined as $R_l = V_{\text{ave}}\Delta t$. It is noted that $V_{\text{ave}}$ represents the average speed of $D$ within the time duration $\Delta t = (t_c - t_p)$. Within the limited region (i.e., the *Request Zone* determined by $S$), the LAR-Box algorithm follows similar procedures as the DSR protocol to choose the appropriate intermediate nodes $N_i$ for packet forwarding. The efficiency for route search can be increased with the constrained area of packet flooding.

## III. VAR Protocol

It will be shown in this section that the knowledge of the destination node's predicted motion is required in the design of the VAR algorithm. The algorithm is designed by considering the following two types of motion prediction models.

### A. Mobility Models

In this subsection, two mobility models, i.e., the GMM model and the CSM model, are presented. These two mobility models will be utilized as two separate cases to predict the MN's movement in the design of the proposed VAR routing algorithm.

*1) GMM Model:* The GMM model [34] is adapted in this paper to represent the motion of each MN. The moving direction $\alpha_k$ (with respect to the positive $x$-axis) and the speed $V_k$ of each MN at a discrete time instant $t_k$ can be formulated as [35]

$$\alpha_k = \gamma_1\alpha_{k-1} + (1-\gamma_1)\bar{\alpha} + \sqrt{(1-\gamma_1^2)}X_{\alpha_{k-1}} \tag{1}$$

$$V_k = \gamma_2 V_{k-1} + (1-\gamma_2)\bar{V} + \sqrt{(1-\gamma_2^2)}X_{V_{k-1}} \tag{2}$$

where $\bar{\alpha}$ and $\bar{V}$ represent the asymptotic mean of the moving direction and the speed as $t_k \to \infty$; $X_{\alpha_{k-1}}$ and $X_{V_{k-1}}$ are the zero-mean Gaussian-distributed random variables; and $\gamma_1$ and $\gamma_2$ are tunable parameters that represent different levels of randomness as $0 \le \gamma_i \le 1$ for $i = 1$ and 2. The two extreme cases correspond to the linear motion (as $\gamma_i = 1$) and the Brownian motion (as $\gamma_i = 0$). The benefit of using the GMM model for the MN's movement is that it preserves certain levels of 1) motion randomness and 2) memories from previous time steps as the parameter $\gamma_i$ varies. A more realistic motion trajectory can be obtained with the GMM model compared with the Random Walk Mobility Model [36], which results in sharp turns and sudden stops. With (1) and (2), the position $P(x_k, y_k)$ of the MN at time instant $t_k$ becomes

$$x_k = x_{k-1} + V_{k-1}\delta t\cos\alpha_{k-1} \tag{3}$$

$$y_k = y_{k-1} + V_{k-1}\delta t\sin\alpha_{k-1} \tag{4}$$

where $\delta t$ is the sampling interval between the time instant $t_k$ and its previous time instant $t_{k-1}$. It is assumed that the position information of an MN, including its position $P(x_i, y_i)$, velocity $V_i$, and heading angle $\alpha_i$, is obtained at time instant $t_i$ via its positioning system. $P(x_j, y_j)$ is the predicted position of the MN at time instant $t_j$ as $t_j \ge t_i$. The traveling distance along the $x$ and $y$ directions (i.e., $\Delta x_{i,j}$ and $\Delta y_{i,j}$) of the MN within the time duration $\Delta t_{i,j} = (t_j - t_i)$ can be obtained by summing along both directions from (3) and (4) as

$$\Delta x_{i,j} = \sum_{k=i+1}^{j} V_k\delta t\cos\alpha_k \tag{5}$$

$$\Delta y_{i,j} = \sum_{k=i+1}^{j} V_k\delta t\sin\alpha_k. \tag{6}$$

It is noted that $\alpha_k$ and $V_k$ represent the moving direction and speed of $D$ at the time instant $t_k$, which can be obtained from (1) and (2).

*2) CSM Model:* In the previous subsection, the GMM model is utilized to obtain the predicted information (including the speed $V_j$ and the moving direction $\alpha_j$) of an MN based on its previous motion states. However, in some cases, it is possible to assume that the MN remains a constant speed $(V_o)$ along the same moving direction $(\alpha_o)$ within the time interval $\Delta t_{i,j} = (t_j - t_i)$, i.e., $V(t) = V_o$ and $\alpha(t) = \alpha_o$ for $t \in [t_i, t_j]$. The traveling distance of the MN along the $x$ and $y$ directions within the time duration $\Delta t_{i,j}$ can therefore be simplified from (5)

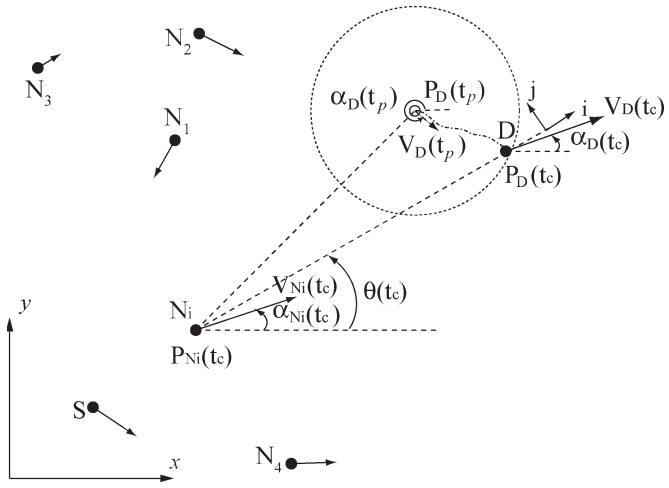


Fig. 1. Schematic of the VAR scheme using the GMM model.

and (6) as

$$\Delta x_{i,j} = V_o \Delta t_{i,j} \cos \alpha_o \tag{7}$$

$$\Delta y_{i,j} = V_o \Delta t_{i,j} \sin \alpha_o. \tag{8}$$

The constant speed assumption in the CSM model is applicable while the MN moves in a constant speed (along with the same direction) manner. This scenario is possible to happen in constrained topologies with similar traffic flows, including city streets and highway topologies. With the constant speed assumption, the CSM model provides a less-expensive computation cost compared with the GMM model. The CSM model is treated as a special case for simple motion prediction. The routing performance of the VAR algorithm using the CSM model will be compared with that using the GMM model in the simulations.

### *B. VAR Algorithm*

In this section, the proposed VAR algorithm is presented. The proposed algorithm determines the feasible MNs for packet forwarding based on the relative velocity between the forwarding node $N_i$ and the destination node $D$. The VAR algorithm is designed by predicting the motion of $D$ using either the GMM model or the CSM model, as shown in the next two subsections.

*1) VAR Using the GMM Model (VAR-GMM):* Fig. 1 shows the schematic of the VAR algorithm using the GMM model. The source node $S$ initiates a route discovery process to the destination node $D$ via some of the intermediate nodes $N_i$. After beaconing within the neighborhood of $S$, an $RREQ$ packet is sent to an intermediate node $N_i$ at the time instant $t_c$. The location information of $N_i$, including its position $P_{N_i}(t_c)$, velocity $V_{N_i}(t_c)$, and heading angle $\alpha_{N_i}(t_c)$, is obtained from its positioning system at the current time instant $t_c$. On the other hand, the location information of $D$ [i.e., $P_D(t_p)$, $V_D(t_p)$, and $\alpha_D(t_p)$] was obtained by $S$ at a previous time instant $t_p$ and was forwarded to $N_i$ via the $RREQ$ packet. By adopting the GMM model, the current location information of $D$ [i.e., $P_D(t_c)$, $V_D(t_c)$, and $\alpha_D(t_c)$] can therefore be calculated from the previous time instant $t_p$ using (1)–(4).

The main concept of the VAR algorithm is to compare the velocity information between the intermediate node $N_i$ with that of $D$ while the $RREQ$ packet has arrived in $N_i$ at the current time $t_c$. The proposed VAR algorithm utilizes the following two criterions to determine if the intermediate node $N_i$ is suitable as the *forwarding node* for packet delivery. The first criterion [as in (9)] of the VAR algorithm indicates that the potential *forwarding node* $N_i$ should move toward the destination node $D$ along their connecting line (i.e., the $i$th direction as shown in Fig. 1), while the second criterion [as in (10)] is used to limit the relative speed between $N_i$ and $D$ along their perpendicular direction $j$, i.e.,

$$\Delta V_i > \left[V_{N_i}(t_c) + V_D(t_c)\right] \delta_{1,i} + \delta_{2,i} \tag{9}$$

$$|\Delta V_j| < \left[V_{N_i}(t_c) + V_D(t_c)\right] \delta_{1,j} + \delta_{2,j} \tag{10}$$

where

$$\begin{aligned} \Delta V_i = {} & V_{N_i}(t_c) \cos\left(\theta(t_c) - \alpha_{N_i}(t_c)\right) \\ & - V_D(t_c) \cos\left(\theta(t_c) - \alpha_D(t_p)\right) \end{aligned} \tag{11}$$

$$\begin{aligned} \Delta V_j = {} & V_{N_i}(t_c) \sin\left(\theta(t_c) - \alpha_{N_i}(t_c)\right) \\ & - V_D(t_c) \sin\left(\theta(t_c) - \alpha_D(t_p)\right). \end{aligned} \tag{12}$$

As shown in Fig. 1, $\theta(t_c)$ represents the angle between $D$ and $N_i$ at $t_c$, which can be calculated as

$$\theta(t_c) = \tan^{-1} \frac{\left[y_D(t_p) - y_{N_i}(t_c)\right] + (\Delta y_{p,c})_D}{\left[x_D(t_p) - x_{N_i}(t_c)\right] + (\Delta x_{p,c})_D} \tag{13}$$

where the location information $(x_D(t_p), y_D(t_p))$ of $D$ is obtained from the positioning system at the previous time instant $t_p$, and the location $(x_{N_i}(t_c), y_{N_i}(t_c))$ of $N_i$ is acquired at the current time $t_c$. Both $(\Delta y_{p,c})_D$ and $(\Delta x_{p,c})_D$ can be obtained by using (5) and (6). It is also noted that $\delta_{1,i}$, $\delta_{2,i} \geq 0$ and $\delta_{1,j}$, $\delta_{2,j} > 0$ in (9) and (10) are the tuning parameters for the VAR criterions. $\delta_{1,i}$ and $\delta_{1,j}$ are utilized to represent the speed-dependent tuning coefficients. With the VAR criterions, the amount of potential *forwarding nodes* within the constrained flooding area will decrease.

*2) VAR Using the CSM Model (VAR-CSM):* As described in Section III-A2, it is feasible to assume the MN to pertain to a constant speed during the time interval $(t \in [t_p, t_c])$ in consideration. The VAR criterions [i.e., (9)–(12)] proposed in the previous subsection are still applicable to be adopted in the CSM model. The only difference is that a simplified version of $\theta_s(t_c)$ is obtained as shown in Fig. 2, i.e.,

$$\theta_s(t_c) = \tan^{-1} \frac{\left[y_D(t_p) - y_{N_i}(t_c)\right] + V_D(t_p) \Delta t_{p,c} \sin \alpha_D(t_p)}{\left[x_D(t_p) - x_{N_i}(t_c)\right] + V_D(t_p) \Delta t_{p,c} \cos \alpha_D(t_p)} \tag{14}$$

where $\Delta t_{p,c} = (t_c - t_p)$. It can be seen that the computation complexity of $\theta_s(t_c)$ is much less than the $\theta(t_c)$ obtained from (13). In the simulation section, the performance comparison between the VAR-GMM and the VAR-CSM schemes will be conducted under different simulation mobility models.

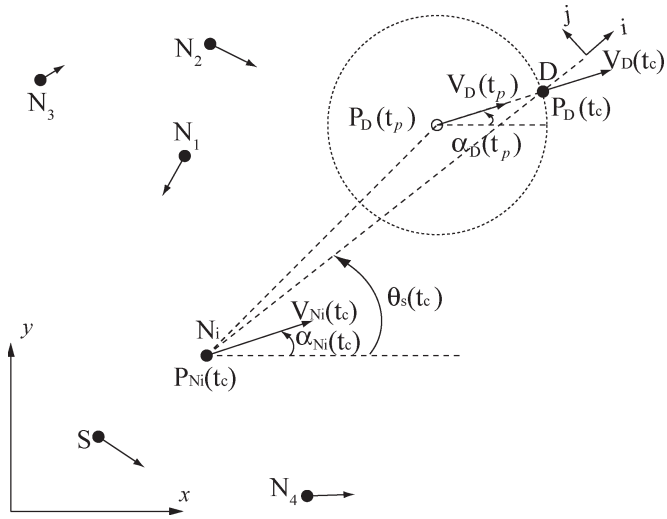


Fig. 2. Schematic of the VAR scheme using the CSM model.

## IV. PMLAR Protocol

The proposed PMLAR protocol will be explained in this section. The first subsection describes the three phases of the PMLAR protocol in detail. The second subsection presents the PMLAR algorithm with the assistance of the VAR scheme, i.e., the PMLAR-V protocol. The PMLAR-LV scheme is addressed in the third subsection, which incorporates a local repair mechanism within the PMLAR-V method. The fourth subsection incorporates a proactive feedback information from $D$ to $S$ within the PMLAR-V algorithm to improve the routing efficiency, i.e., the PMLAR-PV protocol. The following list of parameters denotes the timing variables that will be utilized in the PMLAR protocols:

- $t_{l,s}^{(n)}$ time instant while sending the $LREQ$ packet for the $n$th route request;
- $t_{l,f}^{(n)}$ time instant while receiving the $LREP$ packet for the $n$th route request;
- $t_{r,s}^{(n)}$ time instant while sending the $RREQ$ packet for the $n$th route request;
- $t_{r,f}^{(n)}$ time instant while receiving the $RREP$ packet for the $n$th route request;
- $t_{p,s}^{(n)}$ starting time instant while delivering data packets for the $n$th route request;
- $t_{p,f}^{(n)}$ ending time instant while delivering data packets for the $n$th route request;
- $t_{e}^{(n)}$ time instant while receiving the $RERR$ packet for the $n$th route request;
- $t_{m}^{(n)}$ time instant while receiving the proactive maintenance packet for the $n$th route request.

### A. PMLAR Protocol

Fig. 3 shows the schematic of the network topology with the proposed PMLAR protocol. The PMLAR algorithm is designed for $S$ to predict the current and future location of $D$ to achieve efficient data transmission. An enhanced location service is also considered in the proposed algorithm to address the potential indirect route (IR) between $S$ and $D$. The three phases of

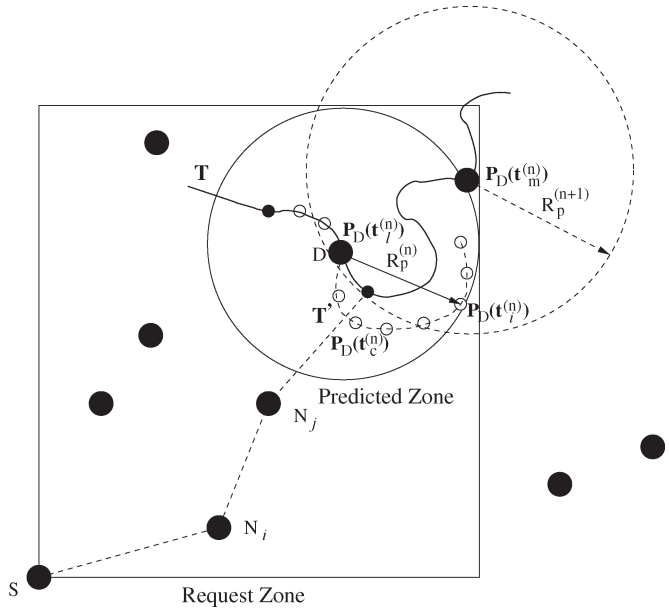


Fig. 3. Schematic of the network topology with the PMLAR protocol.

the PMLAR algorithm (i.e., the location service, the route discovery and packet forwarding, and the route repair phases) are stated as follows.

*1) Location Service:* The source node $S$ intends to transmit data packets to the destination node $D$. However, $S$ has no knowledge about the position information of $D$ at the beginning. It is required for $S$ to activate a location service to obtain the position information of $D$. As shown in Fig. 4, the location service request packet $(LREQ_p^{(n)})$ initiated by $S$ at time $t_{l,s}^{(n)}$ is transmitted to its neighboring MNs using the flooding mechanism, i.e.,

$$LREQ_p^{(n)} = \langle Adr_S, Adr_D \rangle \tag{15}$$

where the superscript $(n)$ denotes the $n$th route request, and the subscript $p$ represents the PMLAR protocol. The parameters $Adr_S$ and $Adr_D$ denote the addresses of nodes $S$ and $D$. After rebroadcasting by the intermediate node $N_i$, $D$ is informed that a position request has been initiated by $S$. It is assumed that the position information of $D$ is updated at the time instant $t_l^{(n)}$, where $t_l^{(n)} = \{t \in \Re | 0 < t \leq t_{l,f}^{(n)}\}$. The up-to-date information of $D$, including the time stamp $t_l^{(n)}$, position $P_D(t_l^{(n)})$, velocity $P_D(t_l^{(n)})$, moving angle $\alpha_D(t_l^{(n)})$, and parameters $\gamma_{iD}(t_l^{(n)})$ (for $i = 1$ and 2), is sent back to $S$ via the reverse route. Moreover, the position information of the forwarding nodes $N_i$, i.e., $\mathbf{P}_{N_i}(t_l^{(n)}) = [P_{N_1}(t_l^{(n)}), \ldots, P_{N_n}(t_l^{(n)})]$, is also transmitted back to $S$. The positions of the intermediate nodes $\mathbf{P}_{N_i}(t_l^{(n)})$ will be utilized in the route discovery phase to determine if an indirect region for packet forwarding is examined. The location service reply packet $(LREP_p^{(n)})$ is received by $S$ at time $t_{l,f}^{(n)}$ while the location information of $D$ is available, i.e.,

$$LREP_p^{(n)} = \left\langle Adr_S, Adr_D, P_D\left(t_l^{(n)}\right), V_D\left(t_l^{(n)}\right) \right.$$
$$\left. \alpha_D\left(t_l^{(n)}\right), \gamma_{iD}\left(t_l^{(n)}\right), \mathbf{P}_{N_i}\left(t_l^{(n)}\right) \right\rangle. \tag{16}$$

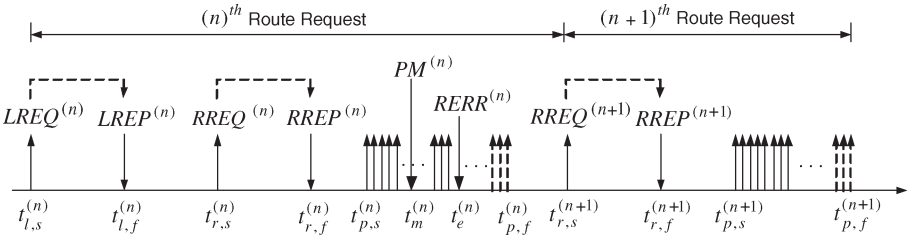


Fig. 4. Timing diagram of the source node $S$ using the PMLAR protocol and its derivative schemes.

It is noted that the two tunable parameters of $D$, $\gamma_{iD}(t_l^{(n)})$ are computed and acquired at time instant $t_l^{(n)}$. As discussed in Section III-A, $\gamma_{1D}$ and $\gamma_{2D}$ represent the level of randomness for the corresponding moving angle $(\alpha_k)$ and speed $(V_k)$ of $D$. To facilitate solving these two parameters, both (1) and (2) can be combined and rewritten into the following format:

$$\underline{y}_k = \mathbf{H}_k \underline{\gamma}_k + \underline{v}_k \tag{17}$$

where

$$\underline{y}_k = \begin{bmatrix} \alpha_k \\ V_k \end{bmatrix}, \quad \mathbf{H}_k = \begin{bmatrix} \alpha_{k-1} & \bar{\alpha} & 0 & 0 \\ 0 & 0 & V_{k-1} & \bar{V} \end{bmatrix}$$

$$\underline{\gamma}_k = \begin{bmatrix} \gamma_{1k} \\ 1-\gamma_{1k} \\ \gamma_{2k} \\ 1-\gamma_{2k} \end{bmatrix}, \quad \underline{v}_k = \begin{bmatrix} \sqrt{(1-\gamma_1^2)} X_{\alpha_{k-1}} \\ \sqrt{(1-\gamma_2^2)} X_{V_{k-1}} \end{bmatrix}.$$

The state vector $\underline{y}_k$ contains the moving direction $\alpha_k$ and speed $V_k$ of $D$ at time instant $t_k$. $\mathbf{H}_k$ is the design matrix for parameter estimation, while $\underline{\gamma}_k$ represents the state vector for the time-varying parameters $\gamma_1$ and $\gamma_2$ of $D$ at time $t_k$. $\underline{v}_k$ denotes the system noises that are scaled from the random variables $X_{\alpha_{k-1}}$ and $X_{V_{k-1}}$. The two parameters $\gamma_1$ and $\gamma_2$ can be estimated at each time instant $t_k$ (i.e., $\hat{\underline{\gamma}}_k$) by solving the state (17) using the recursive least square (RLS) estimation [38], [39] as

$$\hat{\underline{\gamma}}_{k+1} = \hat{\underline{\gamma}}_k - \mathbf{K}_{k+1}\left(\mathbf{H}_{k+1}\hat{\underline{\gamma}}_k - \underline{y}_{k+1}\right) \tag{18}$$

with

$$\mathbf{K}_{k+1} = \mathbf{P}_{k+1}\mathbf{H}_{k+1}^T$$

$$\mathbf{P}_{k+1} = \frac{1}{\lambda}\left[\mathbf{P}_k - \frac{\mathbf{P}_k\mathbf{H}_{k+1}^T\mathbf{H}_{k+1}\mathbf{P}_k}{\lambda + \mathbf{H}_{k+1}\mathbf{P}_k\mathbf{H}_{k+1}^T}\right].$$

It is noted that the tunable parameter $\lambda$ determines the convergence rate of the RLS method. The appropriate values of $\lambda$ under different mobility environments will be determined in the simulation section. As the parameters $\hat{\gamma}_{1D}$ and $\hat{\gamma}_{2D}$ are obtainable with online adaptation, the prediction mechanism can forecast the future position of $D$ based on the state information.

*2) Route Discovery and Packet Forwarding:* $S$ can start the processes of route discovery and forwarding of data packets after executing the location service. The prediction mechanism utilized in the proposed PMLAR algorithm is for $S$ to predict the trajectory of $D$ from its previous location update. As shown in Fig. 3, the trajectory $\mathbf{T}$ (i.e., the sold path) shows the actual moving path of $D$, while $\mathbf{T}'$ (i.e., the dotted path) indicates the predictive path of $D$ starting from the time instant $t_l^{(n)}$. As mentioned in the previous subsection, $t_l^{(n)}$ corresponds to the time instant that the location information of $D$ is acquired from the positioning system. The current and future positions of $D$ can be obtained at different predictive time steps as $\Delta T_l^{(n)} = \kappa \Delta t_l^{(n)} = \kappa(t_{r,s}^{(n)} - t_l^{(n)})$, where $t_{r,s}^{(n)}$ corresponds to the current time instant for initiating a route request packet $(RREQ_p^{(n)})$. As $\kappa = 1$, the current position of $D$ is obtained, while the future position of $D$ is predicted if $\kappa > 1$. The prediction mechanism of the PMLAR protocol defines a *Predicted Zone* based on the predicted trajectory of $D$, as illustrated in Fig. 3. The *Predicted Zone* is defined as a circular region centered at $P_D(t_l^{(n)})$ with its radius $R_p^{(n)}$ defined as

$$R_p^{(n)} = \max_{0<i\le\zeta}\left\{[(\Delta x_{l,i})_D]^2 + [(\Delta y_{l,i})_D]^2\right\}^{\frac{1}{2}} \tag{19}$$

where $(\Delta x_{l,i})_D$ and $(\Delta y_{l,i})_D$ can be obtained from (5) and (6), and $\zeta = \Delta T_l^{(n)}/\delta t$ represents the total number of predicting steps. The distances from $P_D(t_l^{(n)})$ to the position of the $i$th predicting step $P_D(t_i^{(n)})$ are calculated, and the maximum value is selected as the radius of the *Predicted Zone*. As shown in Fig. 3, the predicting mechanism starts at the time instant $t_l^{(n)}$, and the predicting trajectory by using the GMM model is shown in dotted line with empty circles. The number of predicting steps $\zeta$ is equal to 7 in this case. The radius $R_p^{(n)}$ represents the predicted radius that happens at the fifth steps, as in Fig. 3. Similar to the *Expected Zone* as in the LAR-Box algorithm, the *Predicted Zone* defines a circle that predicts the potential movement of the destination node $D$. However, the determination of the *Predicted Zone* is based on the predictive moving behavior of $D$, while the LAR-Box algorithm assumes a constant moving speed of $D$ along the time interval in consideration.

As the *Predicted Zone* is computed by $S$, either the direct routing (DR) or the IR type will be determined. The parameter $\mu$ [as in (20), shown at the bottom of the next page] is utilized to examine the types of routing that is going to be applied, where the position information of $D$ and the intermediate nodes are acquired from $LREP_p^{(n)}$, as in (16). The parameter $\mu$ is utilized to represent the ratio of the routing distances to the connecting line between $S$ and $D$. Two cases are considered as follows.

1) If $\mu \le \mu_t$ (where $\mu_t$ is a prespecified threshold), the DR type of routing is utilized. Similar to the LAR-Box algorithm, a rectangular region, which encloses $S$'s position

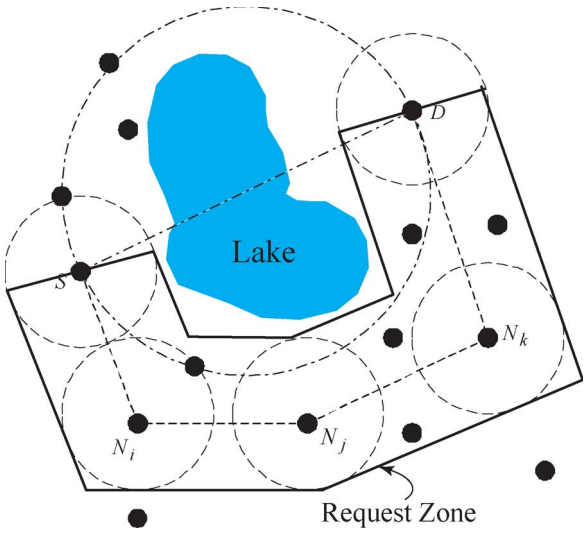


Fig. 5. Schematic of the PMLAR algorithm with the IR scheme.

and the circle of radius $R_p^{(n)}$, is determined, as shown in Fig. 3. The Request Zone $(RZ_{p-\mathrm{DR}}^{(n)})$ can be obtained as

$$RZ_{p-\mathrm{DR}}^{(n)} = \Gamma_{\mathrm{DR}}\left(P_S\left(t_{r,s}^{(n)}\right), P_D\left(t_l^{(n)}\right), R_p^{(n)}\right) \quad (21)$$

where the function $\Gamma_{\mathrm{DR}}(\cdot)$ defines the rectangular area for the DR type of routing.

2) If $\mu > \mu_t$, the IR type of routing will be adopted. A different type of Request Zone for the IR type is illustrated in Fig. 5. The positions of the intermediate nodes [i.e., $\mathbf{P}_{N_i}(t_l^{(n)})$] are utilized as the waypoints for the confined region. The Request Zone $(RZ_{p-IR}^{(n)})$ for the IR type of routing [defined by the function $\Gamma_{IR}(\cdot)$] is obtained as

$$RZ_{p-IR}^{(n)} = \Gamma_{IR}\left(P_S\left(t_{r,s}^{(n)}\right), P_D\left(t_l^{(n)}\right), R_p^{(n)}, \mathbf{P}_{N_i}\left(t_l^{(n)}\right)\right). \quad (22)$$

After the process of location services, $S$ initiates a route discovery process to $D$ via some of the intermediate nodes $N_i$. An $RREQ_p^{(n)}$ packet will be sent out by $S$ to an intermediate node $N_i$ at the time instant $t_{r,s}^{(n)}$ as

$$RREQ_p^{(n)} = \begin{cases} \left\langle Adr_S, Adr_D, RZ_{p-\mathrm{DR}}^{(n)} \right\rangle, & \text{for } \mu \le \mu_t \\ \left\langle Adr_S, Adr_D, RZ_{p-IR}^{(n)} \right\rangle, & \text{for } \mu > \mu_t \end{cases} \quad (23)$$

where the types of Request Zone (i.e., either $RZ_{p-\mathrm{DR}}^{(n)}$ or $RZ_{p-IR}^{(n)}$) selected in the $RREQ_p^{(n)}$ packet will depend on the magnitude of the parameter $\mu$. It is utilized for the intermediate MN to determine if it itself is located within the confined region. After the route to $D$ is established with the appropriate selection of the forwarding MNs, an $RREP_p^{(n)}$ packet is returned to $S$ at time $t_{r,f}^{(n)}$ as

$$RREP_p^{(n)} = \left\langle Adr_S, \{Adr_{N_i}\}, Adr_D, P_D\left(t_r^{(n)}\right) V_D\left(t_r^{(n)}\right), \alpha_D\left(t_r^{(n)}\right), \gamma_{iD}\left(t_r^{(n)}\right)\right\rangle \quad (24)$$

where $\{Adr_{N_i}\}$ denotes the addresses for the set of intermediate MNs that are selected as the forwarding nodes within the route. The additional information of $D$ [including $P_D(t_r^{(n)})$, $V_D(t_r^{(n)})$, $\alpha_D(t_r^{(n)})$, and $\gamma_{iD}(t_r^{(n)})$] is also delivered back to $S$ via the $RREP_p^{(n)}$ packet, where $t_r^{(n)} = \{t \in \Re | t_l^{(n)} < t \le t_{r,f}^{(n)}\}$ represents the time instant that the location information is updated at $D$. Thereafter, the source node $S$ will utilize the route obtained from the $RREP_p^{(n)}$ packet to transmit data packets to $D$ between the time instants $t_{p,s}^{(n)}$ and $t_{p,f}^{(n)}$.

*3) Route Repair:* Due to the dynamic changes of network topologies, route maintenance and repair should take place during data transmission from $S$ to $D$. The proposed PMLAR algorithm provides a repairing mechanism for broken transmission links.

Similar to the route error repairing capability as in the DSR protocol [4], the source node $S$ receives a route error $(RERR_p^{(n)})$ packet from one of the forwarding MNs if there exists a broken transmission link in the originally defined route. As shown in Fig. 4, the link is broken at the time instant $t_e^{(n)}$, where $t_e^{(n)} = \{t \in \Re | t_{p,s}^{(n)} < t < t_{p,f}^{(n)}\}$ happens between the duration of data packet transmission. A new route discovery process [i.e., the $(n+1)$th route request] will be initiated by $S$. The source node $S$ will define a new Request Zone (i.e., either $RZ_{p-\mathrm{DR}}^{(n+1)}$ or $RZ_{p-IR}^{(n+1)}$) as the confined region to select the appropriate MNs for packet forwarding. A new set of route request/reply process will be adopted, which is followed by the remaining data packet transmission.

### B. PMLAR Protocol With VAR Scheme (PMLAR-V)

The prediction mechanism, as described in the PMLAR protocol, defines the *Predicted Zone* that predicts the potential future position of the destination node $D$. All of the intermediate nodes within the Request Zone (as shown in Fig. 3) are considered as potential forwarding nodes to transmit date packets, e.g., node $N_i$, $N_j$, or $N_k$. However, it is possible to further impose additional constraints on the selection of the intermediate nodes. Since the velocity information of the MNs is available from most of the positioning systems, it is reasonable to incorporate the MN's velocity information as an additional

$$\mu = \frac{\left\|P_{N_1}\left(t_l^{(n)}\right) - P_S\left(t_{r,s}^{(n)}\right)\right\| + \sum_{k=1}^{n-1}\left\|P_{N_{k+1}}\left(t_l^{(n)}\right) - P_{N_k}\left(t_l^{(n)}\right)\right\| + \left\|P_D\left(t_l^{(n)}\right) - P_{N_n}\left(t_l^{(n)}\right)\right\|}{\left\|P_D\left(t_l^{(n)}\right) - P_S\left(t_{r,s}^{(n)}\right)\right\|} \quad (20)$$

criterion to determine if the MN is a feasible node for packet forwarding from $S$ to $D$. A new route request ($RREQ_{p-v}^{(n)}$) packet will be sent out by $S$ at time $t_{r,s}^{(n)}$ to initiate the route discovery process. By combining the location information of $D$ [including $P_D(t_l^{(n)})$, $V_D(t_l^{(n)})$, and $\alpha_D(t_l^{(n)})$] that was obtained from the $LREP_p^{(n)}$ packet [as in (16)], the original route request ($RREQ_p^{(n)}$) packet [as in (23)] is extended as that in (25), shown at the bottom of the page, where the subscript $p-v$ denotes the PMLAR-V algorithm. After receiving the $RREQ_{p-v}^{(n)}$ packet from $S$, $N_i$ will perform the VAR algorithm [based on the criterions in (9) and (10)] to determine if it itself is a suitable node for packet forwarding. If the VAR criterions are satisfied, $N_i$ will record itself within the routing information on the $RREQ_{p-v}^{(n)}$ packet header and rebroadcast the packet to $N_j$. The destination node $D$ is informed that a request for data transmission is initiated by $S$ after receiving the $RREQ_{p-v}^{(n)}$ packet. $D$ will send out the route reply ($RREP_{p-v}^{(n)}$) packet to $S$ via the reverse route, which is recorded on the $RREQ_{p-v}^{(n)}$ packet header. The $RREP_{p-v}^{(n)}$ is returned to $S$ at time $t_{r,f}^{(n)}$ as $RREP_{p-v}^{(n)} = \langle RREP_p^{(n)} \rangle$, where $RREP_p^{(n)}$ is defined as in (24). After completing the route discovery process, the data packets can be delivered from $S$ to $D$ via the designated route. As shown in Fig. 3, the route is selected to comply with both the prediction mechanism and the VAR algorithm.

It is noted that in the original VAR algorithm, the route request packet is flooded to all regions for route discovery, where they seek for intermediate nodes that satisfy the criterions as in (9) and (10). With the limited searching area within the Request Zone in the PMLAR-V algorithm, the inefficiency occurring from the all-region flooding can be improved. The selection of the potential forwarding nodes can therefore be confined within the predefined region.

### C. PMLAR Protocol With VAR and Local Repair Schemes (PMLAR-LV)

In this subsection, a local repair mechanism is adopted within the PMLAR-V scheme to improve the overhead induced by the original repairing process. Assuming that the route for packet delivery has been constructed as $RT = \{S, \ldots, N_i, N_j, \ldots, D\}$, the link between nodes $N_i$ and $N_j$ is considered broken due to the dynamic movements of the MNs. In the original route repair scheme (as stated in Section IV-A3), the source node $S$ will receive a route error ($RRER_p^{(n)}$) packet from node $N_i$, and a new route will be discovered and initiated by node $S$ for further data transmission. In the local repair scheme, node $N_i$ is considered as the source node after it receives the route error message. Node $N_i$ will start to initiate the route request packet targeting to the destination node, which now becomes node $N_j$. Therefore, the route request/reply process will be locally conducted between nodes $N_i$ and $N_j$ instead of the end-to-end route repair (between nodes $S$ and $D$), as in the original scheme. The performance of the PMLAR-LV scheme by adopting the local repair mechanism will be evaluated in the simulation section.

### D. PMLAR Protocol With VAR and Proactive Maintenance Schemes (PMLAR-PV)

This subsection introduces a mechanism for proactive route maintenance before the linkage within a route is likely to break. The prediction mechanism of the destination node $D$ monitors its own position to ensure that it will stay within the *Predicted Zone*, i.e., the circle shown in Fig. 3. The prediction mechanism periodically observes the updated position of $D$ from the positioning system to verify if $D$ is still located within the boundary of the *Predicted Zone*. If $D$ moves close to (or goes out of) the boundary at time instant $t_m^{(n)}$, the mechanism for proactive maintenance within $D$ will be initiated. As shown in Fig. 3, $P_D(t_m^{(n)})$ indicates the position of $D$ that is close to the boundary of the circle with radius $R_p^{(n)}$. The updated information of $D$, including $t_m^{(n)}$, $P_D(t_m^{(n)})$, $V_D(t_m^{(n)})$, $\alpha_D(t_m^{(n)})$, and $\gamma_{iD}(t_m^{(n)})$, is sent back to $S$ using the reversed data transmission route (i.e., within the $PM^{(n)}$ packet, as shown in Fig. 4). $S$ will initiate a new route discovery process with the $RREQ_{p-pv}^{(n+1)}$ packet, which is similar to (25) but with the updated information of $D$ at time $t_m^{(n)}$. The subscript of $RREQ_{p-pv}^{(n+1)}$ denotes a PMLAR protocol with the VAR and proactive maintenance schemes.

It is noted that both $RZ_{p-\mathrm{DR}}^{(n+1)}$ and $RZ_{p-IR}^{(n+1)}$, which are defined in the $RREQ_{p-pv}^{(n+1)}$ packet, rely on the newly generated *Predicted Zone*, i.e., the dotted circle with radius $R_p^{(n+1)}$, as shown in Fig. 3. The proposed PMLAR-PV protocol provides the mechanism for $D$ to update its current information to $S$ if it moves toward the boundary of the *Predicted Zone*. The proactive update scheme can effectively increase the communication robustness within the delivering route. The performance of the proposed algorithms (including the VAR, PMLAR, PMLAR-V, PMLAR-LV, and PMLAR-PV schemes) will be simulated and evaluated in the next section.

## V. Performance Evaluation

### A. Mobility Model

Different types of MN's mobility affect the performance of the designed *ad hoc* routing algorithms. It is therefore important to construct feasible mobility models that emulate the realistic moving environment for simulation purposes. The RWM model

$$RREQ_{p-v}^{(n)} = \begin{cases} \left\langle Adr_S, Adr_D, RZ_{p-\mathrm{DR}}^{(n)}, P_D\left(t_l^{(n)}\right), V_D\left(t_l^{(n)}\right), \alpha_D\left(t_l^{(n)}\right) \right\rangle, & \text{for } \mu \le \mu_t \\ \left\langle Adr_S, Adr_D, RZ_{p-IR}^{(n)}, P_D\left(t_l^{(n)}\right), V_D\left(t_l^{(n)}\right), \alpha_D\left(t_l^{(n)}\right) \right\rangle, & \text{for } \mu > \mu_t \end{cases} \tag{25}$$

is widely used to evaluate the performance of *ad hoc* routing protocols [13], [14], [36]. Each MN moves toward a randomly selected destination node with a chosen speed. The MN pauses for a preselected timeout period and resumes its movement again. The MN's speed and timeout period are tunable parameters to simulate different moving environments.

In this paper, an HM model is developed to evaluate the effectiveness of the proposed algorithms in simulations. The following scenarios are considered in the proposed HM model to closely emulate real traffic environments (such as highways and city streets).

1) A bidirectional four-lane street (two lanes in each direction) is assumed in the HM model.
2) In the moving directions (i.e., MNs move along the $x$ direction at the lower two lanes and along the $-x$ direction at the upper two lanes), the MNs should maintain their speeds based on an average speed, which is prespecified for each lane.
3) The MNs may deviate within the lane for a certain degree in the lateral direction (i.e., along the $y$ direction).
4) Lane changes are allowed in the HM model. If the speed of the MN at the slow (fast) lane is larger (smaller) than a predefined value, the MN should start the lane-changing process.

The HM model that satisfies the above traffic scenarios can be formulated by modifying from the GMM model, as described in Section III-A. In the HM model, the motion equation of MNs along the $x$ direction is represented by $x_k$, as in (3). The associated $V_k$ is obtained from (2), where $\bar{V}$ is selected based on the average speed of each lane. The moving direction $\alpha_k$ should be confined to the lane direction with small variations due to different driving behaviors. $\alpha_v$ can be modified from (1) by setting $\gamma = 0$ as

$$\alpha_k = \bar{\alpha} + X_{\alpha_{k-1}} \tag{26}$$

where $\bar{\alpha} = 0$ (or $\pi$) for moving along the positive (or negative) $x$ direction. The zero-mean Gaussian-distributed random variable $X_{\alpha_{k-1}}$ is varied based on a preassumed driving deviation. The lateral displacement $y_k$ can be modified from (4) as

$$y_k = y_0 + V_{k-1}\delta t \sin\alpha_{k-1} \tag{27}$$

where $y_0$ is a constant value (i.e., $y_0 = y_{\text{slow}}$ for the slow lane and $y_0 = y_{\text{fast}}$ for the fast lane), depending on the initial position of the MN along the $y$ direction. The reason of using a constant $y_0$ is to simulate the driving behavior of maintaining the MN along the center of a lane.

Fig. 6 shows the state diagram for the lane-changing scenarios. The probability distribution function of the MN's speed $V_k$ is denoted as $f_{V_k}(v)$, where $V_k$ is a Gaussian-distributed random variable [as can be observed from (2)]. To satisfy the conditions for lane change, the following cumulative distribution functions (cdfs) are defined.

1) $F_1(v) = f_{V_k}[V_k > V_{\text{upper}}] = \int_{V_{\text{upper}}}^{\infty} f_{V_k}(v)dv$: $F_1(v)$ is the cdf when the MN's speed $V_k$ is greater than the upper speed threshold $V_{\text{upper}}$. As shown in Fig. 6, the MN will move to the fast lane if it is currently in the slow lane.

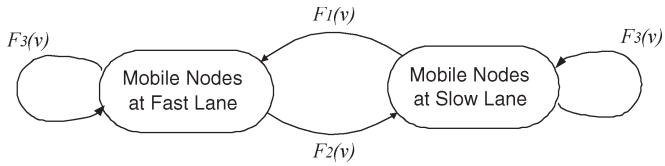


Fig. 6. State diagram for lane-changing scenario.

2) $F_2(v) = f_{V_k}[V_k < V_{\text{lower}}] = \int_{-\infty}^{V_{\text{lower}}} f_{V_k}(v)dv$: $F_2(v)$ is the cdf when the MN's speed $V_k$ is smaller than the lower speed threshold $V_{\text{lower}}$. The MN will move to the slow lane if it is currently in the fast lane.
3) $F_3(v) = f_{V_k}[V_{\text{lower}} \le V_k \le V_{\text{upper}} = \int_{V_{\text{lower}}}^{V_{\text{upper}}} f_{V_k}(v)\,dv$: $F_3(v)$ is the cdf when the MN's speed $V_k$ lies between the lower and upper speed limits. The MN will remain in its current state.

Both the RWM model and the HM model will be utilized in the simulations to evaluate the performance of the proposed algorithms in the following subsections.

### B. Simulation Parameters

The simulations were conducted using the Network Simulator (ns-2, [37]) to compare the proposed VAR, PMLAR, PMLAR-V, PMLAR-LV, and PMLAR-PV algorithms with the existing LAR-Box and DSR protocols. There are 70 MNs existing in the network with a total of ten constant bit rate connections in the simulations. The results are obtained by averaging the 100 simulation runs for 500 s. The average speeds of the MNs selected in the simulations are 5, 10, 15, and 20 m/s. The velocity thresholds that are utilized in (9) and (10) are assigned as $\delta_{1i} = 0.125$, $\delta_{2i} = 0.5$, $\delta_{1j} = 0.25$, and $\delta_{2j} = 0.5$. It is noted that $\delta_{1i}$ and $\delta_{1j}$ are selected smaller compared with $\delta_{2i}$ and $\delta_{2j}$ since they will both be multiplied by the velocity variables in the criterions. Moreover, $\delta_{1i}$ and $\delta_{2i}$ are chosen such that $\Delta V_i$ is greater than a positive value, which indicates that the selected node $N_i$ should move toward the destination node $D$. The relative perpendicular speeds between $N_i$ and $D$ (i.e., $\Delta V_j$) should fall within the upper and lower bounds as determined by $\delta_{1j}$ and $\delta_{2j}$. It is also found in the simulation results that the performance evaluation of the VAR-based schemes is not sensitive to these four velocity thresholds.

The threshold $\mu_t$ is selected as $\pi/2$ for determining if the DR or IR types of routing should be utilized. For the IR type of routing to happen (as shown in Fig. 5), $\mu > \mu_t = (\pi\overline{SD}/2)/(\overline{SD}) = \pi/2$ indicates that the lower bound for the accumulated routing distances between the MNs is selected as half of the circle perimeter with diameter equal to $\overline{SD}$, where $\overline{SD}$ is the direct distance between $S$ and $D$. To validate the effectiveness of the proposed algorithms, the following three types of mobility models are utilized in the simulations with their parameters.

1) RWM model: The RWM model is adopted within the simulation area of $500 \times 500$ m$^2$. The MNs' average pause time is set at 5 s.
2) RWM-IR model: The RWM-IR model is utilized in the simulations, as shown in Fig. 7. There exist an unreachable area of $300 \times 300$ m$^2$ within the simulation area of

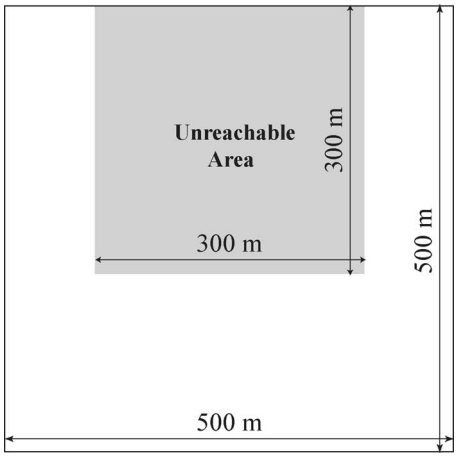


Fig. 7. Simulation model for the IR scenario.

$500 \times 500$ m$^2$. The IR type of routing as described in the PMLAR protocol will be validated using this scenario. The MNs' average pause time is also set at 5 s.

3) HM model: The HM model is adopted with four straight lanes (two lanes in each direction), each being 3.2 km in length and 4 m in width. The average speed of the MNs in the fast lanes is 4 m/s greater than that in the slow lanes. The variance of $X_{\alpha_{k-1}}$ for each MN is chosen to be 3°.

### C. Parameter Estimation

As mentioned in Section III-B, the parameters $\gamma_i$'s are adapted online based on the RLS method [as in (17) and (18)]. To provide a fast converging RLS method, a proper selection of the parameter $\lambda$ is required. In this subsection, the appropriate selection of $\lambda$ is determined based on the different moving behaviors within the RWM and HM models.

*1) Parameter Estimation for the RWM Model:* As mentioned in Section V-A, the RWM model primarily consists of 1) a constant speed motion along the arbitrary direction and 2) a stationary speed motion for a prespecified time interval. The moving behaviors of the RWM model can be represented by the GMM model, which possesses both 1) high randomly selected moving angles [i.e., smaller values of $\gamma_1$ in (1)] and 2) switching movements between constant speed and stationary motions [i.e., alternating between larger and smaller values of $\gamma_2$ in (2)]. Therefore, the behaviors of the RWM model can be emulated by the GMM model that is utilized within the proposed schemes. The main purpose of this subsection is to offline obtain and validate the tunable parameter $\lambda$ within the RLS method such that the RWM model can be emulated by the GMM model with its parameters $\hat{\gamma}_i$ adapted online.

Several parameters in the GMM model are prespecified to offline emulate the corresponding RWM model. For validation purposes, the parameters in (1) are selected as $(\gamma_1, \bar{\alpha}, X_{\alpha_{k-1}}) = (a, 360 \cdot \zeta \cdot rand(0,1), \mathcal{N}(0,10))$ for $t = \{t \in \Re | (\zeta - 1) \cdot t_{s2} \le t \le \zeta \cdot t_{s2}, \zeta > 0\}$. The parameter $\gamma_1$ is assigned $a = (0.0, 0.1, 0.2)$ as the three different simulation cases shown in Fig. 8. The relative low values of $\gamma_1$ are selected to reflect that the moving angles $\alpha_k$ mostly depend on the average angle

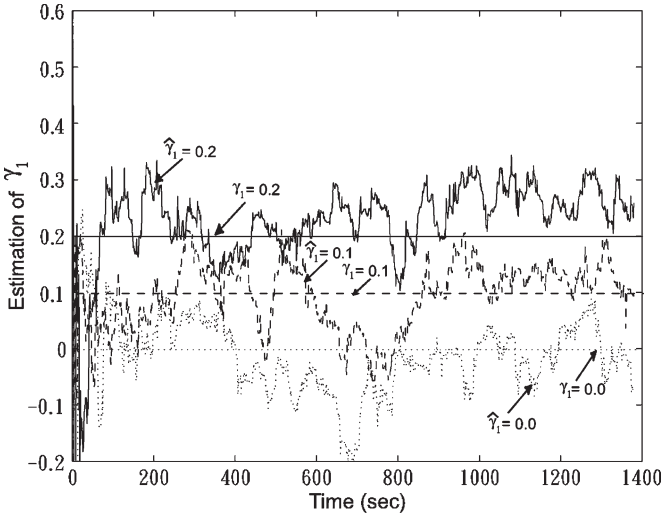


Fig. 8. Parameter estimation $\hat{\gamma}_1$ for the RWM model with $\lambda = 0.9755$ (solid line: estimation for $\gamma_1 = 0.2$; dashed line: estimation for $\gamma_1 = 0.1$; and dotted line: estimation for $\gamma_1 = 0.0$).

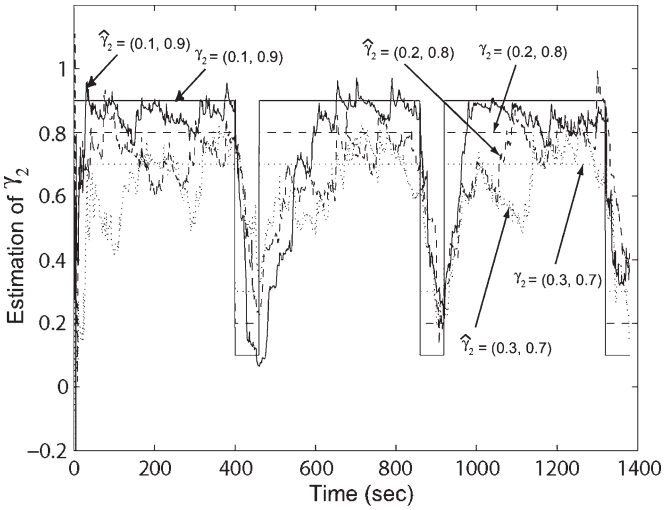


Fig. 9. Parameter estimation $\hat{\gamma}_2$ for the RWM model with $\lambda = 0.9755$ [solid line: estimation for $\gamma_2 = (0.1, 0.9)$; dashed line: estimation for $\gamma_2 = (0.2, 0.8)$; and dotted line: estimation for $\gamma_2 = (0.3, 0.7)$].

$\bar{\alpha}$ and the corresponding variations. The $\zeta$th $\bar{\alpha}$ is randomly selected based on the different time interval $\zeta \cdot t_{s2}$, where $t_{s2}$ is chosen as 460 s in the simulations. As illustrated in Fig. 8, the three types of lines (i.e., solid, dashed, and dotted lines) represent different values of $\gamma_1$ to be estimated using the RLS method. For example, the curved solid line stands for the estimated $\hat{\gamma}_1$, which attempts to track the straight solid line with $\gamma_1 = 0.2$. Several values of the parameter $\lambda$ have been experimented to offer better tracking ability for the validation models. It is found that $\lambda = 0.9755$ can provide satisfactory tracing performance compared with the other $\lambda$ values.

As shown in Fig. 9, the parameters in (2) are selected as $(\gamma_2, \bar{V}, X_{V_{k-1}}) = ((b,c), (10,0), \mathcal{N}(0,2))$, where

$$\gamma_2 = \begin{cases} b, & \text{for } (\zeta - 1) \cdot t_{s2} \le t \le \zeta \cdot t_{s1} + (\zeta - 1) \cdot t_{s2} \\ c, & \text{for } \zeta \cdot t_{s1} + (\zeta - 1) \cdot t_{s2} \le t \le \zeta \cdot t_{s2} \end{cases}. \tag{28}$$

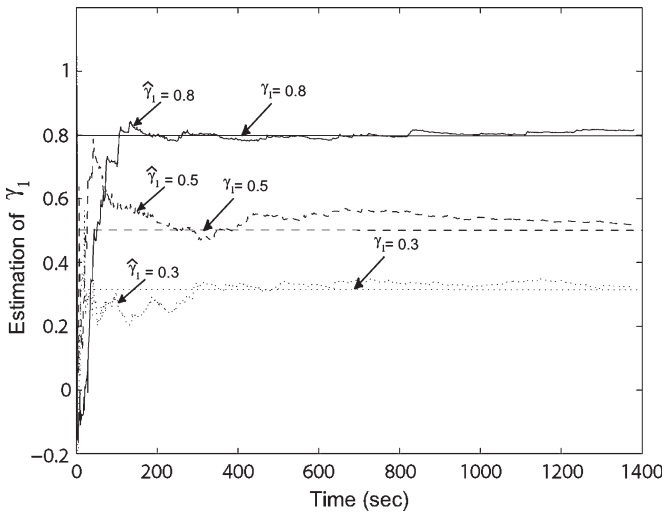


Fig. 10. Parameter estimation $\hat{\gamma}_1$ for the HM model with $\lambda = 0.9999$ (solid line: estimation for $\gamma_1 = 0.8$; dashed line: estimation for $\gamma_1 = 0.5$; and dotted line: estimation for $\gamma_1 = 0.3$).

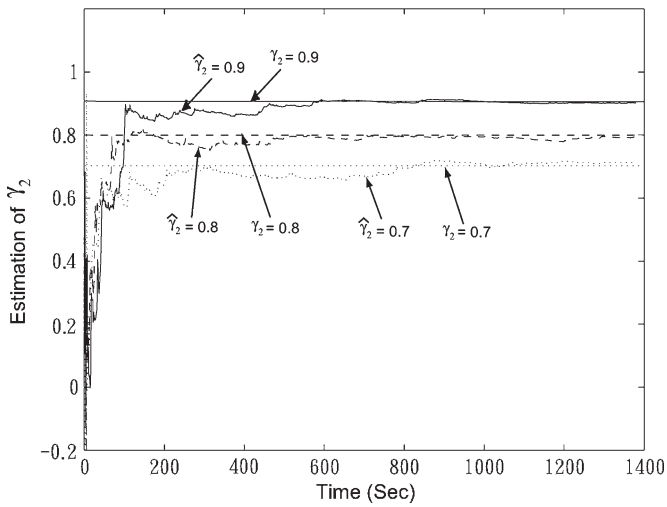


Fig. 11. Parameter estimation $\hat{\gamma}_2$ for the HM model with $\lambda = 0.9999$ (solid line: estimation for $\gamma_2 = 0.9$; dashed line: estimation for $\gamma_2 = 0.8$; and dotted line: estimation for $\gamma_2 = 0.7$).

It is noted that $t_{s1} = 400$ s and $t_{s2} = 460$ s are selected in the simulations, as in Fig. 9. The three cases are represented by the variations of the parameter $\gamma_2 = (b, c) = (0.9, 0.1), (0.8, 0.2)$, and (0.7, 0.3). The value $b$ of $\gamma_2$ represents the time intervals where comparably linear movement of the RWM model is assumed (with $\bar{V} = 10$ m/s), while $\gamma_2 = c$ indicates the time intervals that the MNs are relatively stationary ($\bar{V} = 0$ m/s) with less dependency to their previous moving behaviors. The selection of the two different values of $\gamma_2$ is attempting to emulate the movement of the RWM model, i.e., the MNs move in constant speeds and then pause for a certain time period. It is also evaluated in the simulations that $\lambda = 0.9755$ (as shown in Fig. 9) provides acceptable tracking performance compared with the other values. The value of $\lambda = 0.9755$ will be utilized as the simulation parameter, while the RWM model is used as the underlying mobility model in the simulations.

*2) Parameter Estimation for the HM Model:* Similar to the discussion in the previous subsection, the parameter $\lambda$ within the RLS method is acquired offline using the GMM model to emulate the corresponding HM model. The parameters in (1) are selected as $(\gamma_1, \bar{\alpha}, X_{\alpha_{k-1}}) = (a, 0, \mathcal{N}(0, 10))$. The parameter $\gamma_1$ is chosen as $a = (0.3, 0.5, 0.8)$ as the three different simulation cases, as in Fig. 10. The values of $\gamma_1$ are selected to reflect the moving angles that are selected depending the driving behaviors, which can either be randomly selected (i.e., $\gamma_1 = 0.3$) or linearly related to previous driving manners (i.e., $\gamma_1 = 0.8$). It is found in the simulations that $\lambda = 0.9999$ is sufficient for the estimated $\hat{\gamma}_1$ to trace the various $\gamma_1$ values, i.e., for $\gamma_1 = 0.8, 0.5$, and $0.3$, as illustrated in Fig. 10.

The parameters in (2) are selected as $(\gamma_2, \bar{V}, X_{V_{k-1}}) = (b, \zeta \cdot rand(5, 25), \mathcal{N}(0, 2))$ for $t = \{t \in \Re | (\zeta - 1) \cdot t_{s2} \leq t \leq \zeta \cdot t_{s2}, \zeta > 0\}$. The parameter $\gamma_2$ is assigned $b = (0.7, 0.8, 0.9)$ as the three different cases, as illustrated in Fig. 11. The relatively high values of $\gamma_2$ are selected to reflect that constant speeds are preserved under highway driving. The average speed of each MN is changed at certain time instants, where the $\zeta$th $\bar{V}$ is randomly chosen based on the different time interval $\zeta \cdot t_{s2}$. The value of $t_{s2}$ is also selected as 460 s in the simulations. As shown in Fig. 11, adequate tracking performance can be obtained for the estimated $\hat{\gamma}_2$ by selecting $\lambda = 0.9999$, which is the same value as in the selection of $\hat{\gamma}_1$ for the HM model. The value of $\lambda = 0.9999$ is adopted as the parameter, while the HM model is utilized as the underlying mobility model in the simulations.

### D. Simulation Results

The following four metrics are considered for performance comparison:

1) The Data Packet Delivery Ratio: the percentage of successful deliveries for the data packets;
2) The End-to-End Delay: the average time elapsed for delivering a data packet from the transmitter to the receiver;
3) The Control Packet Overhead: the ratio from the total transmitted control packets to the total received data packets;
4) The Route Life Time: the average life time of a route for data transmission.

With the simulation parameters and the performance comparison metrics stated above, the simulation results are explained in the following two subsections.

*1) Performance Comparison Between the VAR-GMM and the VAR-CSM Algorithms:* In this subsection, the performance comparison for the VAR algorithm using either the GMM or the CSM model is evaluated. Figs. 12–14 show the performance comparison for both VAR-GMM and VAR-CSM algorithms that are implemented under the RWM and HM models (with $V = 5, 10, 15, 20$ m/s). It can be observed that the VAR-GMM algorithm outperforms the VAR-CSM scheme under both RWM and HM models in all the three comparison metrics.

As illustrated in Fig. 12, the data packet delivery ratio of the VAR-GMM algorithm is around 2%–3% higher than that of the VAR-CSM scheme under both mobility models. The end-to-end delay of the VAR-GMM algorithm is around 40–50 ms less, compared with the VAR-CSM scheme at $V = 20$ m/s (as in Fig. 13). The control packet overhead of the VAR-GMM

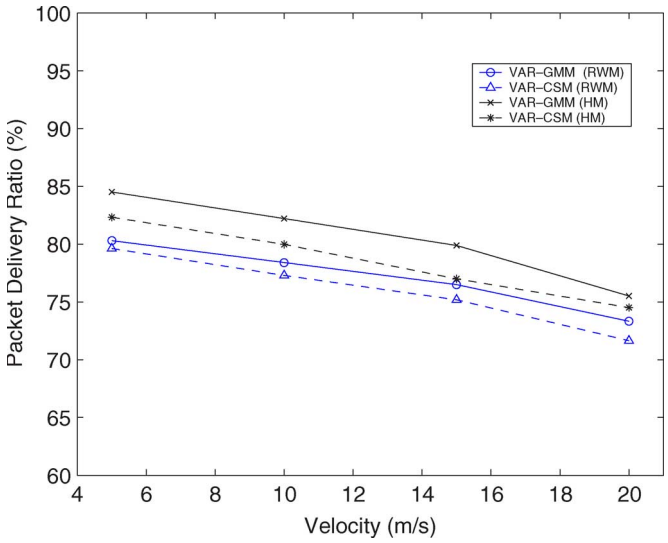


Fig. 12. Data packet delivery ratio versus average velocity for both VAR-GMM and VAR-CSM algorithms under RWM and HM models.

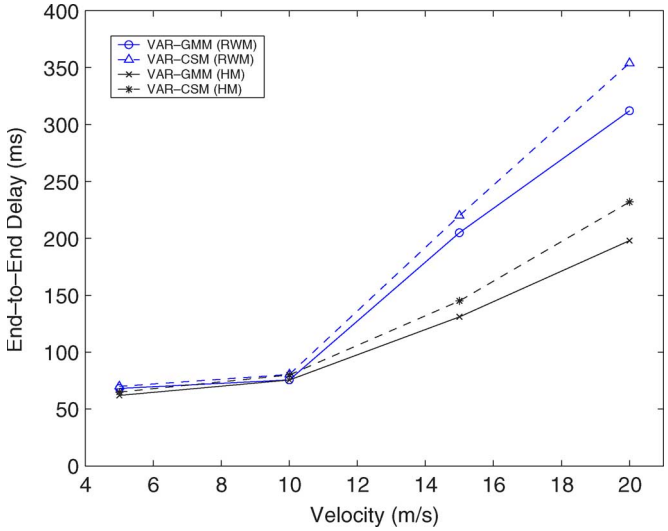


Fig. 13. End-to-end delay versus average velocity for both VAR-GMM and VAR-CSM algorithms under RWM and HM models.

scheme is around 1.5–2 smaller than that using the VAR-CSM algorithm for both mobility models at $V = 20$ m/s (as in Fig. 14). It is noticed that the simulation results as above can be expected since the more accurate is the predicting model used (i.e., the GMM model), the better can the routing performance be obtained. However, the benefit of using the CSM model is that it provides efficiency in algorithm computation compared with the GMM model. It is also observed that the simulation results obtained by using the HM model illustrate better performance compared with that from the RWM model in all three metrics. These results are obtained because the selected simulation scenario for the HM model has better routing efficiency compared with that from the RWM model. In the next subsection, the GMM model is selected as the predicting mechanism for the performance evaluation of the proposed algorithms, including the VAR, PMLAR, PMLAR-V, PMLAR-LV, and PMLAR-PV algorithms.

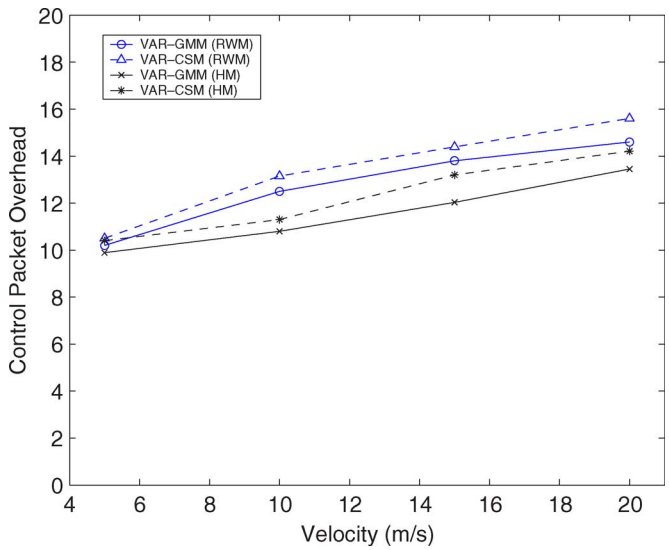


Fig. 14. Control packet overhead versus average velocity for both VAR-GMM and VAR-CSM algorithms under RWM and HM models.

*2) Performance Evaluation of the PMLAR and Its Associated Algorithms:* In this subsection, the performances between the proposed VAR, PMLAR, PMLAR-V, PMLAR-LV, and PMLAR-PV algorithms, and the existing DSR and LAR-Box protocols are compared. It is noted that the GMM model is utilized as the prediction model in all the simulation cases. Figs. 15–18 illustrate the performance comparison under the RWM and RWM-IR models, while the simulation results under the HM model are shown in Figs. 19–22. As seen in Fig. 15, the data packet delivery ratio for the PMLAR-PV algorithm can achieve around 8% and 13% higher ratios than that from the LAR-Box algorithm under the RWM and RWM-IR models (at speed $= 20$ m/s). The PMLAR-derived protocols (i.e., the PMLAR, PMLAR-V, PMLAR-LV, and PMLAR-PV schemes) can acquire a higher packet delivery ratio than the VAR, LAR-Box, and DSR algorithms. It can also be found that the separation between the PMLAR derivative schemes and the non-PMLAR protocols becomes more obvious under the RWM-IR model (as shown in the right plot of Fig. 15). The reason comes from the additional waypoint information that is obtained from the location service while the PMLAR-related schemes are encountering the IR scenarios. This waypoint information helps to direct the route discovery and packet-forwarding processes in the right directions.

Fig. 16 illustrates that the end-to-end delay of the PMLAR-PV scheme is around 180 and 210 ms less, compared with that of the LAR-Box protocol under the RWM and RWM-IR models (at $V = 20$ m/s). It is also worthwhile to notice that the PMLAR scheme can achieve a smaller end-to-end delay compared with the PMLAR-V, PMLAR-LV, and PMLAR-PV algorithms under the RWM-IR model (as shown in the right plot of Fig. 16). It is found in the simulation data that the selection of forwarding MNs based on the relative velocity (i.e., in the PMLAR-V, the PMLAR-LV, and the PMLAR-PV schemes) causes an adverse effect under the RWM-IR model. The selected forwarding MNs that move in the same direction as the destination node may move out of the regions confined

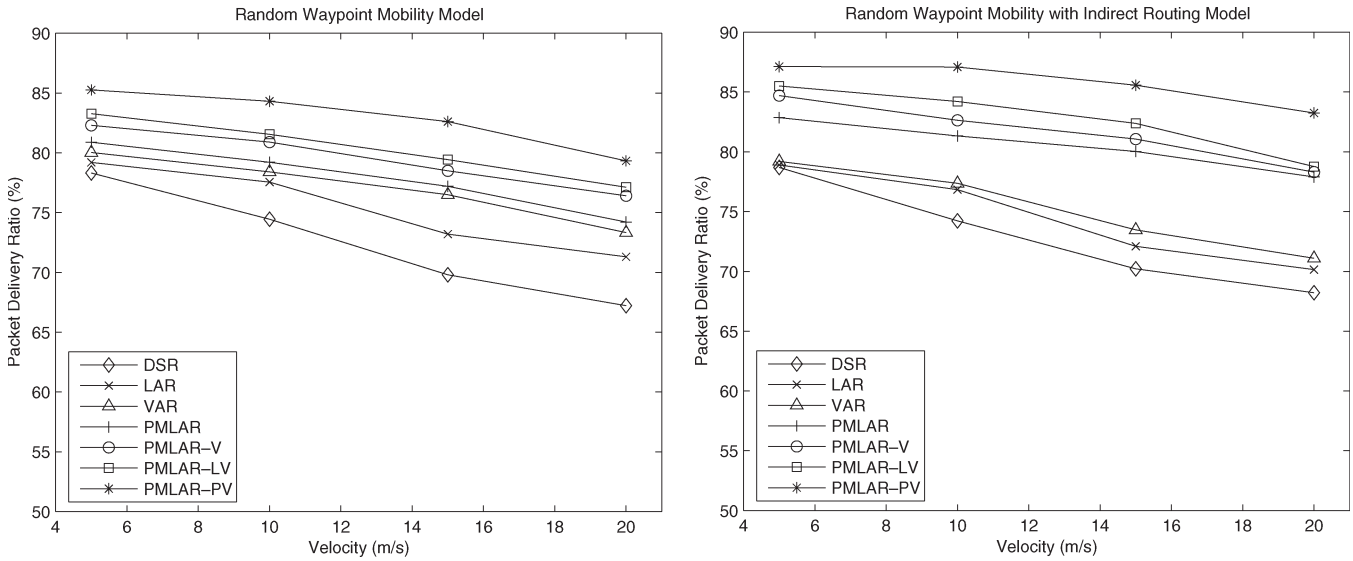


Fig. 15. Packet delivery ratio versus average velocity with the RWM (left plot) and RWM-IR (right plot) models.

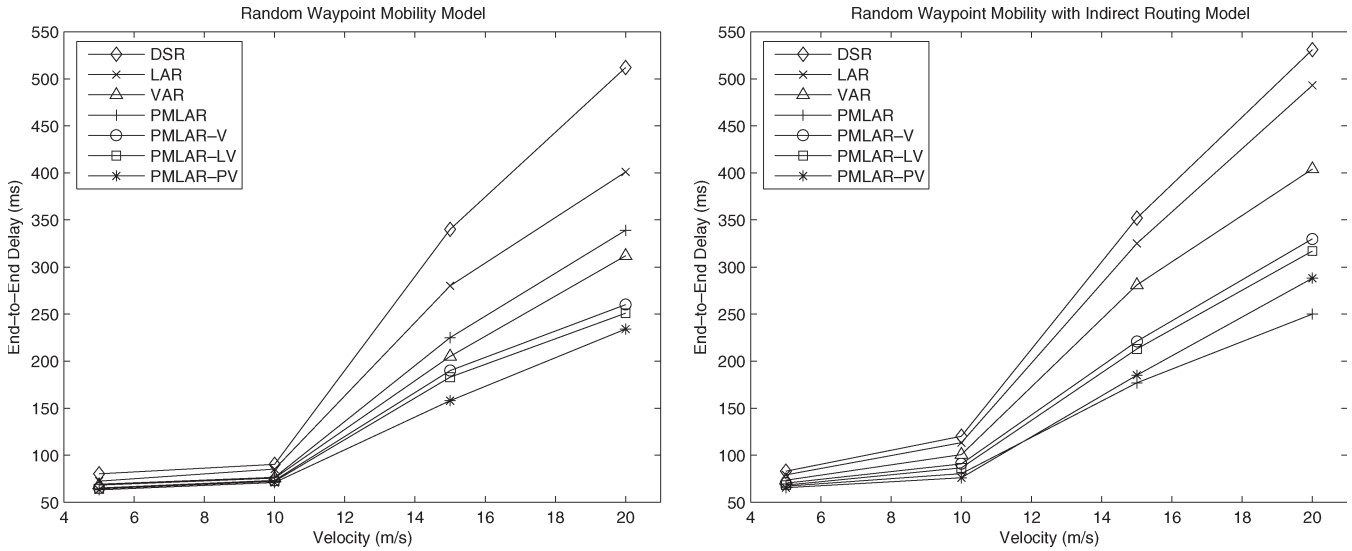


Fig. 16. End-to-end delay versus average velocity with the RWM (left plot) and RWM-IR (right plot) models.

by the waypoints, which can result in potential link breakage for the delivering routes. Nevertheless, the PMLAR-derived schemes still outperform the DSR, LAR-Box, and VAR protocols with smaller end-to-end delay.

Due to the mechanism of proactive route maintenance, the PMLAR-PV scheme contributes more control overhead than the PMLAR, PMLAR-V, and PMLAR-LV algorithms, as shown in Fig. 17. The destination node $D$ periodically monitors its own position to ensure that it will stay within the *Predicted Zone*. If $D$ moves close to the boundary of the region, it will send an update information back to the source node $S$, and a new route discovery process will be initiated by $S$. The information update packets and the new route discovery packets are the causes of additional control overhead. However, the total control overhead of the PMLAR-PV scheme is still lower than that obtained from the DSR, LAR-Box, and VAR protocols. Fig. 18 shows the performance comparison under the average route lifetime metrics. The proposed PMLAR-PV scheme can provide additional 24 and 28 s of average route lifetime compared with that of the LAR-Box algorithm under the RWM and RWM-IR models (at $V = 20$ m/s). It is also observed that comparably robust communication linkages can be obtained using the PMLAR derivative schemes, especially under the RWM-IR model.

From Figs. 15–17, it can be observed that the performance of the PMLAR-LV scheme, which adopts a local route repair, is comparably better than the PMLAR-V algorithm, which utilizes the end-to-end route repair. The localized mechanism decreases the delay time while repairing a route and provides a higher probability for a successful packet delivery. However, it is worthwhile to find that the routes created by the PMLAR-LV scheme tend to become unstable in the high-speed environments. As shown in Fig. 18, the route lifetime of the PMLAR-LV scheme is higher than that from the PMLAR-V method under lower speed environments. However, the decreasing rate from the PMLAR-LV method is comparably larger than

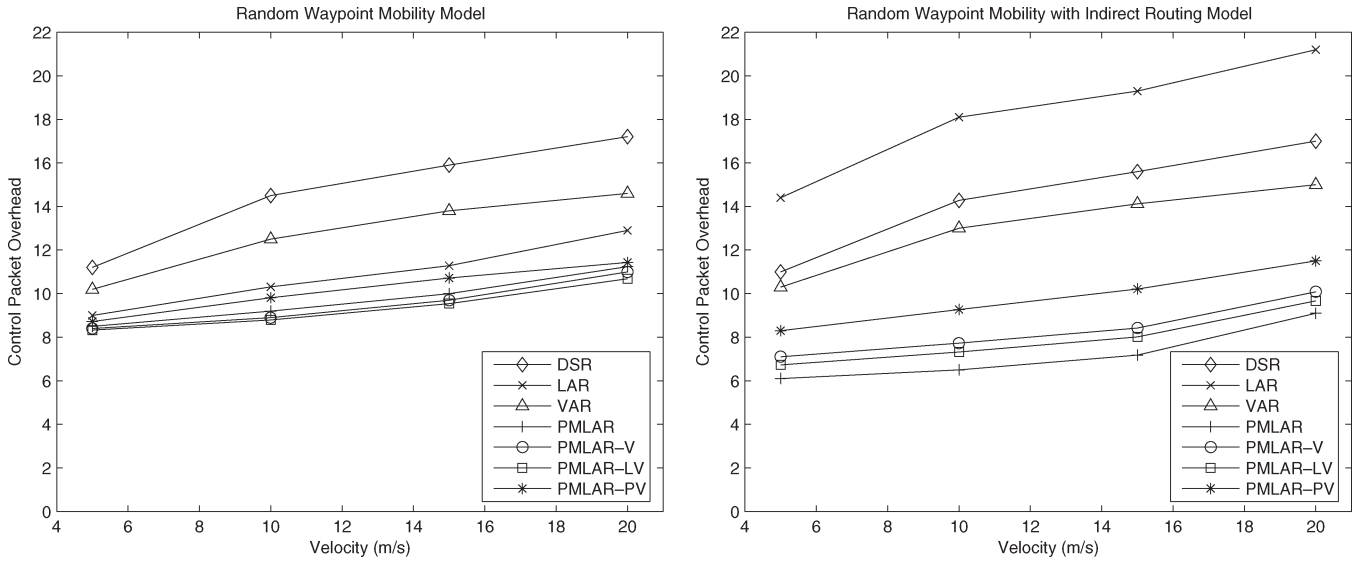


Fig. 17. Control packet overhead versus average velocity with the RWM (left plot) and RWM-IR (right plot) models.

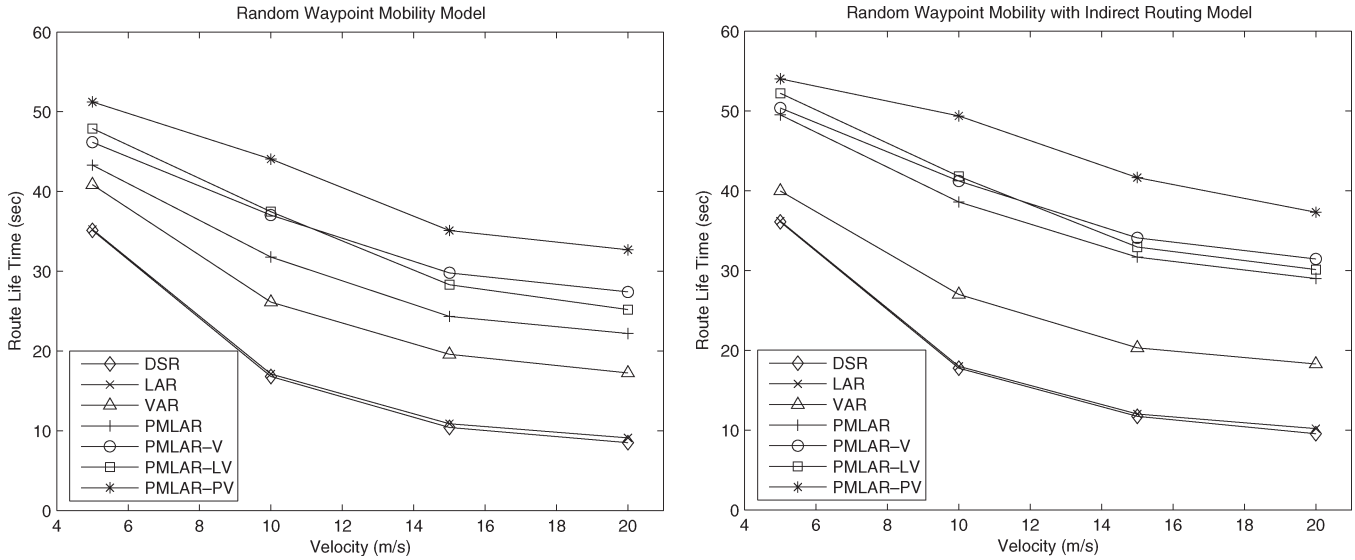


Fig. 18. Route life time versus average velocity with the RWM (left plot) and RWM-IR (right plot) models.

that from the PMLAR-V scheme as the velocity is increased. The primary reason can be attributed to the inferior local route repair under dynamic moving environments. As the speeds of the MNs are increased, the communication links between the MNs are inclined to be broken. The PMLAR-V scheme offers the end-to-end route repair, which has a higher possibility to acquire a more stable route for packet delivery. On the other hand, the PMLAR-LV method provides a localized view for route repair, which may tend to become unstable under high-speed environments. In general, the route lifetime obtained by the PMLAR-PV scheme still outperforms all the other algorithms under various velocities due to its proactive route maintenance.

Moreover, since the LAR-Box protocol can be regarded as the special case of the PMLAR scheme (i.e., by assigning $\gamma_i = 1$ in the GMM prediction model), the PMLAR algorithm and its associated schemes provide better routing performance compared with the LAR-Box protocol. It can also be observed that the performance of the LAR-Box protocol is inferior under the RWM-IR model compared with that under the RWM model (as in Figs. 15–18). Due to the unreachable area within the RWM-IR model, the source node will not be able to construct routes within the rectangular box (i.e., the Request Zone) generated by the LAR-Box protocol. The unreachability problem can be resolved by adopting the additional waypoint information within the PMLAR-related schemes, which can acquire better performance under the three metrics.

In the HM scenario (as in Figs. 19–22), the velocity-based protocols (i.e., the VAR, PMLAR-V, PMLAR-LV, and PMLAR-PV schemes) outperform the nonvelocity-based algorithms (i.e., the PMLAR, LAR-Box, and DSR schemes) in the packet delivery ratio, end-to-end delay, and route lifetime metrics. The similar moving behaviors of the MNs within the HM model cause the velocity-based algorithms to provide better routing efficiency compared with the other schemes. Moreover, the PMLAR-LV method provides a better route

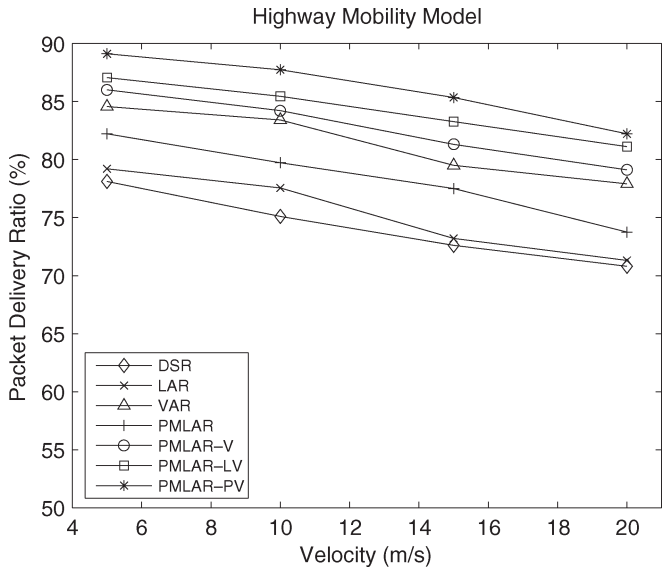


Fig. 19. Packet delivery ratio versus average velocity with the HM model.

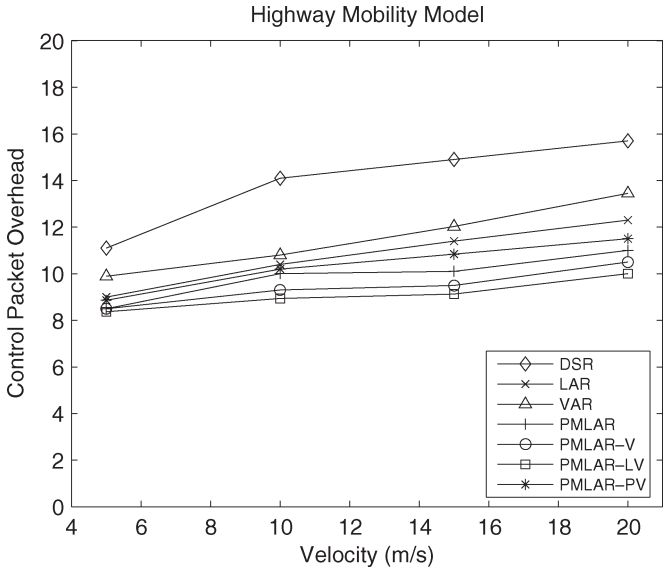


Fig. 21. Control packet overhead versus average velocity with the HM model.

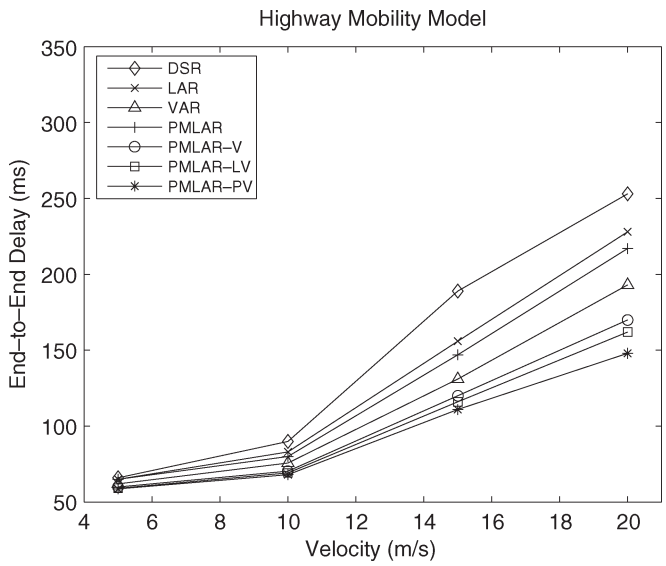


Fig. 20. End-to-end delay versus average velocity with the HM model.

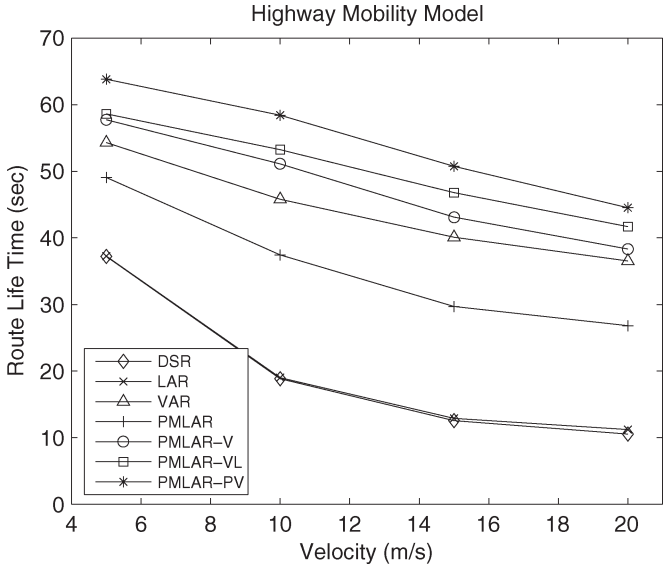


Fig. 22. Route life time versus average velocity with the HM model.

lifetime compared with the PMLAR-V scheme under different speeds. Due to the similar moving behaviors within the HM model, the localized route repair is sufficient to acquire feasible routes in contrast to the end-to-end manner. It can be observed from the simulation results that the PMLAR-PV scheme can still preserve adequate routing performance, i.e., with around 11% higher packet delivery ratio and 90 ms less end-to-end delay compared with the LAR-Box protocol (under the speed of 20 m/s).

Similar results can be obtained in the control overhead metric, as in Fig. 21. The PMLAR-PV algorithm contributes a slightly higher control packet overhead (compared with the PMLAR-V, PMLAR-LV, and PMLAR schemes) due to its proactive route maintenance. It can also be seen that the control packet overhead acquired from the VAR protocol is higher than that from the LAR-Box protocol. The higher overhead comes from the whole-region flooding by the VAR algorithm, while the LAR-Box protocol incurs a comparably smaller overhead by constraining its flooding area within the Request Zone.

## VI. Conclusion

In this paper, the VAR and PMLAR protocols have been proposed for MANETs. The VAR algorithm considers the relative velocity between the intermediate node and the destination node in its protocol design. The PMLAR algorithm is designed with the incorporation of the predictive moving behaviors of the MNs. The prediction mechanism proposed in the PMLAR algorithm can effectively forecast the future trajectory of the destination node. The PMLAR-V scheme enhances the PMLAR protocol with the VAR algorithm, while the local route repair is adopted within the PMLAR-LV scheme. The PMLAR-PV algorithm further encompasses a proactive maintenance scheme in the protocol design. By incorporating the

mobility characteristics in the proposed algorithms, the routing performance can be improved and adapted to different environments. It is shown in the simulations that the proposed PMLAR-PV protocol outperforms other schemes under different network topologies.

## REFERENCES


[1] C. E. Perkins and P. Bhagwat, "Highly dynamic destination sequence distance vector (DSDV) routing for mobile computers," in *Proc. ACM SIGCOMM*, London, U.K., 1994, pp. 234–244.

[2] S. Murthy and J. J. Garcia-Luna-Aceves, "An efficient routing protocol for wireless networks," *ACM Mobile Netw. Appl.*, vol. 1, no. 2, pp. 183–197, Oct. 1996.

[3] C. E. Perkins and E. M. Royer, "Ad-hoc on-demand distance vector routing," in *Proc. 1st IEEE WMCSA*, New Orleans, LA, 1999, pp. 99–100.

[4] D. B. Johnson, D. A. Maltz, and J. Broch, "DSR: The dynamic source routing protocol for multi-hop wireless ad hoc networks," in *Ad Hoc Networking*, C. E. Perkins, Ed. Boston, MA: Addison-Wesley, 2001, pp. 139–172.

[5] V. D. Park and M. S. Corson, "A highly adaptive distributed routing algorithm for mobile wireless networks," in *Proc. 16th Annu. Joint Conf. IEEE INFOCOM*, Kobe, Japan, 1997, pp. 1405–1413.

[6] C.-K. Toh, "A novel distributed routing protocol to support ad-hoc mobile computing," in *Proc. IEEE 15th Annu. IPCCC*, Phoenix, AZ, 1996, pp. 480–486.

[7] R. Dube, C. D. Rais, K.-Y. Wang, and S. K. Tripathi, "Signal stability based adaptive routing (SSA) for ad-hoc mobile networks," *IEEE Pers. Commun.*, vol. 4, no. 1, pp. 36–45, Feb. 1997.

[8] Z. J. Haas and M. R. Pearlman, "The performance of query control schemes for the zone routing protocol," *IEEE/ACM Trans. Netw.*, vol. 9, no. 4, pp. 427–438, Aug. 2001.

[9] P. Samar, M. R. Pearlman, and Z. J. Haas, "Hybrid routing: The pursuit of an adaptable and scalable routing framework for ad hoc networks," in *Handbook of Ad Hoc Wireless Networks*, M. Ilyas, Ed. Boca Raton, FL: CRC, 2003, pp. 245–262.

[10] C.-C. Chiang, H.-K. Wu, W. Liu, and M. Gerla, "Routing in clustered multihop, mobile wireless networks with fading channel," in *Proc. IEEE SICON*, Singapore, 1997, pp. 197–211.

[11] A. Iwata, C.-C. Chiang, G. Pei, M. Gerla, and T.-W. Chen, "Scalable routing strategies for ad hoc wireless networks," *IEEE J. Sel. Areas Commun.*, vol. 17, no. 8, pp. 1369–1379, Aug. 1999.

[12] R. Sivahumar, P. Sinha, and V. Bharghavan, "CEDAR: A core-extraction distributed ad hoc routing algorithm," *IEEE J. Sel. Areas Commun.*, vol. 17, no. 8, pp. 1454–1465, Aug. 1999.

[13] J. Borch, D. Maltz, D. Johnson, Y.-C. Hu, and J. Jetcheva, "A performance comparison of multi-hop wireless ad hoc network routing protocols," in *Proc. 4th Annu. ACM/IEEE Int. Conf. MobiCom*, Dallas, TX, 1998, pp. 25–30.

[14] P. Johansson, T. Larsson, N. Hedman, B. Mielczarek, and M. Degermark, "Routing protocols for mobile ad-hoc networks—A comparative performance analysis," in *Proc. 5th Annu. ACM/IEEE Int. Conf. MobiCom*, Seattle, WA, 1999, pp. 195–206.

[15] E. R. Royer and C.-K. Toh, "A review of current routing protocols for ah hoc mobile wireless networks," *IEEE Pers. Commun.*, vol. 6, no. 2, pp. 46–55, Apr. 1999.

[16] S. R. Das, R. Castaneda, J. Yan, and R. Sengupta, "Comparative performance evaluation of routing protocols for mobile, ad hoc networks," in *Proc. 7th ICCCN*, Lafayette, LA, 1998, pp. 153–161.

[17] Y.-C. Tseng, S.-L. Wu, W.-H. Liao, and C.-M. Chao, "Location awareness in ad hoc wireless mobile networks," *IEEE Trans. Comput.*, vol. 34, no. 6, pp. 46–52, Jun. 2001.

[18] K.-T. Feng and T.-E. Lu, "Velocity and location aided routing for mobile ad hoc networks," in *Proc. IEEE 60th VTC—Fall*, Los Angeles, CA, 2004, pp. 2789–2793.

[19] T.-E. Lu and K.-T. Feng, "Predictive mobility and location-aware routing protocol in mobile ad hoc networks," in *Proc. IEEE GLOBECOM Conf.*, St. Louis, MO, 2005, pp. 899–903.

[20] S. Basagni, I. Chlamtac, V. R. Syrotiuk, and B. A. Woodward, "A distance routing effect algorithm for mobility (DREAM)," in *Proc. 4th Annu. ACM/IEEE Int. Conf. MobiCom*, Dallas, TX, 1998, pp. 76–84.

[21] Y.-B. Ko and N. H. Vaidya, "Location-aided routing (LAR) in mobile ad hoc networks," *ACM Wireless Netw.*, vol. 6, no. 4, pp. 307–321, Jul. 2000.

[22] R. Jain, A. Puri, and R. Sengupta, "Geographical routing using partial information for wireless ad hoc networks," *IEEE Pers. Commun.*, vol. 8, no. 1, pp. 48–57, Feb. 2001.

[23] B. Karp and H. T. Kung, "GPSR: Greedy perimeter stateless routing for wireless networks," in *Proc. 6th Annu. ACM/IEEE Int. Conf. MobiCom*, Boston, MA, 2000, pp. 243–254.

[24] J. Li, J. Jannotti, D. S. J. D. Couto, D. R. Karger, and R. Morris, "A scalable location service for geographic ad hoc routing," in *Proc. 6th Annu. ACM/IEEE Int. Conf. MobiCom*, Boston, MA, 2000, pp. 120–130.

[25] R. Morris, J. Jannotti, F. Kaashoek, J. Li, and D. S. J. D. Couto, "Carnet: A scalable ad hoc wireless network system," in *Proc. 9th ACM SIGOPS Eur. Workshop*, Kolding, Denmark, 2000, pp. 61–65.

[26] B. W. Parkinson and S. W. Gilbert, "NAVSTAR: Global positioning system—Ten years later," *Proc. IEEE*, vol. 71, no. 10, pp. 1177–1186, Oct. 1983.

[27] M. Mauve, J. Widmer, and H. Hartenstein, "A survey on position-based routing in mobile ad-hoc networks," *IEEE Netw.*, vol. 15, no. 6, pp. 30–39, Nov. 2001.

[28] T. Camp, J. Boleng, B. Williams, L. Wilcox, and W. Navidi, "Performance comparison of two location based routing protocols for ad hoc networks," in *Proc. 21st Annu. Joint Conf. IEEE INFOCOM*, New York, 2002, pp. 1678–1687.

[29] P. Yao, E. Krohne, and T. Camp, "Performance comparison of geocast routing protocols for a manet," in *Proc. 13th ICCCN*, Rosemont, IL, 2004, pp. 213–220.

[30] G. Lin, G. Noubir, and R. Rajmohan, "Mobility models for ad hoc network simulation," in *Proc. 23rd Annu. Joint Conf. IEEE INFOCOM*, Hong Kong, 2004, pp. 454–463.

[31] D. Yu and H. Li, "Influence of mobility models on node distribution in ad hoc networks," in *Proc. ICCT*, Beijing, China, 2003, pp. 985–989.

[32] T. Camp, J. Boleng, and V. Davies, "A survey of mobility models for ad hoc network research," *Wireless Commun. Mobile Comput.*, vol. 2, no. 5, pp. 483–502, Aug. 2002.

[33] D. Son, A. Helmy, and B. Krishnamachari, "The effect of mobility-induced location errors on geographic routing in ad hoc networks: Analysis and improvement using mobility prediction," in *Proc. IEEE WCNC*, Atlanta, GA, 2004, pp. 189–194.

[34] A. Gelb, *Applied Optimal Estimation*. Cambridge, MA: MIT Press, 1974.

[35] B. Liang and Z. Haas, "Predictive distance-based mobility management for PCS networks," in *Proc. 18th Annu. Joint Conf. IEEE INFOCOM*, New York, 1999, pp. 1377–1384.

[36] X. Hong, M. Gerla, G. Pei, and C. Chiang, "A group mobility model for ad hoc wireless networks," in *Proc. 2nd ACM Int. Workshop MSWiM*, Seattle, WA, 1999, pp. 53–60.

[37] J. Heidemann, N. Bulusu, J. Elson, C. Intanagonwiwak, K. Lan, Y. Xu, W. Ye, D. Estrin, and R. Govindan, "Effects of detail in wireless network simulation," in *Proc. SCS Multiconference Distrib. Simul.*, Phoenix, AZ, 2001, pp. 3–11.

[38] S. L. J. Marple, *Digital Spectral Analysis With Applications*. Englewood Cliffs, NJ: Prentice-Hall, 1987.

[39] J. C. Spall, *Introduction to Stochastic Search and Optimization: Estimation, Simulation, and Control*. Hoboken, NJ: Wiley, 2003.



**Kai-Ten Feng** (M'03) was born in Taipei, Taiwan, R.O.C., in 1970. He received the B.S. degree from the National Taiwan University, Taipei, in 1992, the M.S. degree from the University of Michigan, Ann Arbor, in 1996, and the Ph.D. degree from the University of California, Berkeley, in 2000.

Between 2000 and 2003, he was an In-Vehicle Development Manager/Senior Technologist with OnStar Corporation USA, a subsidiary of General Motors Corporation, where his major responsibilities included the design of future Telematics platforms and in-vehicle networks. Since February 2003, he has been an Assistant Professor with the Department of Communication Engineering, National Chiao Tung University, Hsinchu, Taiwan. His current research interests include mobile *ad hoc* networks, wireless sensor networks, embedded system design, wireless location technologies, and intelligent transportation systems (ITSs).

Dr. Feng has served on the technical program committees of the Vehicular Technology Society, Asia Pacific Wireless Communications Symposium, and International Conference on Communications, Circuits, and Systems. He received the Best Paper Award from the Spring 2006 IEEE Vehicular Technology Conference, which was ranked as the first among the 615 accepted papers.

**Chung-Hsien Hsu** (S'07) received the B.S. degree in computer and information science from Aletheia University, Taipei, Taiwan, R.O.C., in 2002 and the M.S. degree in computer science and engineering from Tatung University, Taipei, in 2004. He is currently working toward the Ph.D. degree with the Department of Communication Engineering, National Chiao Tung University, Hsinchu, Taiwan.

His current research interests include mac and network-layer issues for mobile *ad hoc* networks, wireless sensor networks, wireless mesh networks, and broadband wireless networks.

**Tse-En Lu** received the B.S. degree in electrical engineering from the National Taiwan University of Science and Technology, Taipei, Taiwan, R.O.C., in 2003 and the M.S. degree in communication engineering from National Chiao Tung University, Hsinchu, Taiwan, in 2005.

He is currently with the Alpha Networks Inc., Hsinchu, where he is responsible for wireless software development. His research interests include wireless communication and mobile *ad hoc* networks.